nature cell biology

Differential effects on lung and bone metastasis of breast cancer by Wnt signalling inhibitor DKK1

Xueqian Zhuang[1], Hao Zhang[1], Xiaoyan Li[2], Xiaoxun Li[1], Min Cong[1], Fangli Peng[1], Jingyi Yu[1], Xue Zhang[1], Qifeng Yang[2,3] and Guohong Hu[1,3]

Metastatic cancer is a systemic disease, and metastasis determinants might elicit completely different effects in various target organs. Here we show that tumour-secreted DKK1 is a serological marker of breast cancer metastasis organotropism and inhibits lung metastasis. DKK1 suppresses PTGS2-induced macrophage and neutrophil recruitment in lung metastases by antagonizing cancer cell non-canonical WNT/PCP–RAC1–JNK signalling. In the lungs, DKK1 also inhibits WNT/Ca^{2+}–CaMKII–NF-κB signalling and suppresses LTBP1-mediated TGF-β secretion of cancer cells. In contrast, DKK1 promotes breast-to-bone metastasis by regulating canonical WNT signalling of osteoblasts. Importantly, targeting canonical WNT may not be beneficial to treatment of metastatic cancer, while combinatory therapy against JNK and TGF-β signalling effectively prevents metastasis to both the lungs and bone. Thus, DKK1 represents a class of Janus-faced molecules with dichotomous roles in organotropic metastasis, and our data provide a rationale for new anti-metastasis approaches.

The majority of breast-cancer-related deaths are attributed to metastasis to distant organs such as the lungs and bone. Previous efforts have identified organ-specific gene signatures and functional molecules of breast cancer metastasis[1–3], highlighting distinct microenvironmental prerequisites for disseminated cancer cells to colonize various organs. However, current studies are usually limited to a selected target organ of metastasis, and the comprehensive roles of metastasis determinants in multiple organs are under-investigated. Metastasis is a systemic disease, and targeted treatment for metastasis of one organ might elicit adverse side effects in other metastasis sites. For instance, bisphosphonates (which are osteoporosis-targeting drugs) effectively reduce bone metastasis while in some conditions may worsen adrenal metastasis of breast cancer[4]. Thus, identification of pluripotent markers for multiple-organ metastasis prognosis, and development of systemic anti-metastasis therapeutics are necessary to reconcile unmet medical needs.

The WNT signalling pathway, consisting of canonical and non-canonical branches, plays prominent roles in development and cancer. Canonical WNT signalling is mediated by β-catenin and activates the TCF/LEF family of transcription factors, while non-canonical WNT/Ca^{2+} and WNT/planar cell polarity (PCP) pathways are independent of β-catenin. The WNT/Ca^{2+} pathway activates calcineurin, Ca^{2+}/calmodulin-dependent protein kinase II (CaMKII) and protein kinase C (PKC), further leading to activation of multiple downstream signalling pathways[5]. The WNT/PCP pathway can activate Rho–ROCK and RAC1–JNK–JUN axes, playing important roles in cytoskeleton regulation[6]. WNT signalling is regulated by multiple extracellular factors, among which Dickkopf-1 (DKK1) binds to the WNT co-receptor LDL-receptor-related protein 5/6 (LRP5/6) and desensitizes cells from canonical WNT ligands[7]. Moreover, DKK1 is also reported to regulate non-canonical WNT signalling, leading to either activation or suppression of the pathways[8–11]. WNT signalling has been well established to be oncogenic for breast cancer[12]. In addition, DKK1 is known to promote osteolytic bone metastasis by regulating osteoclastogenesis[13–16]. However, the roles of DKK1 and WNT signalling in metastasis to other organs are less studied. In particular, the role of non-canonical WNT signalling in metastasis organotropism is not clear. Here we report that tumour-secreted DKK1 suppresses lung metastasis of breast cancer, and plays opposite roles in metastasis organotropism by targeting different WNT signalling branches of different cell populations in multiple metastasis organs.

RESULTS

DKK1 secretion is associated with breast cancer metastasis organotropism

To comprehensively investigate tumour-secreted proteins, which often play important roles in metastasis microenvironment regulation, we performed mass-spectrum secretome profiling of the MDA-MB-231

[1]The Key Laboratory of Stem Cell Biology, Institute of Health Sciences, Shanghai Institutes for Biological Sciences, Chinese Academy of Sciences & Shanghai Jiao Tong University School of Medicine, University of Chinese Academy of Sciences, Shanghai 200031, China. [2]Department of Breast Surgery, Qilu Hospital of Shandong University, Ji'nan 250012, China.
[3]Correspondence should be addressed to Q.Y. or G.H. (e-mail: qifengy_sdu@163.com or ghhu@sibs.ac.cn)

Received 16 September 2016; accepted 14 August 2017; published online 11 September 2017; DOI: 10.1038/ncb3613

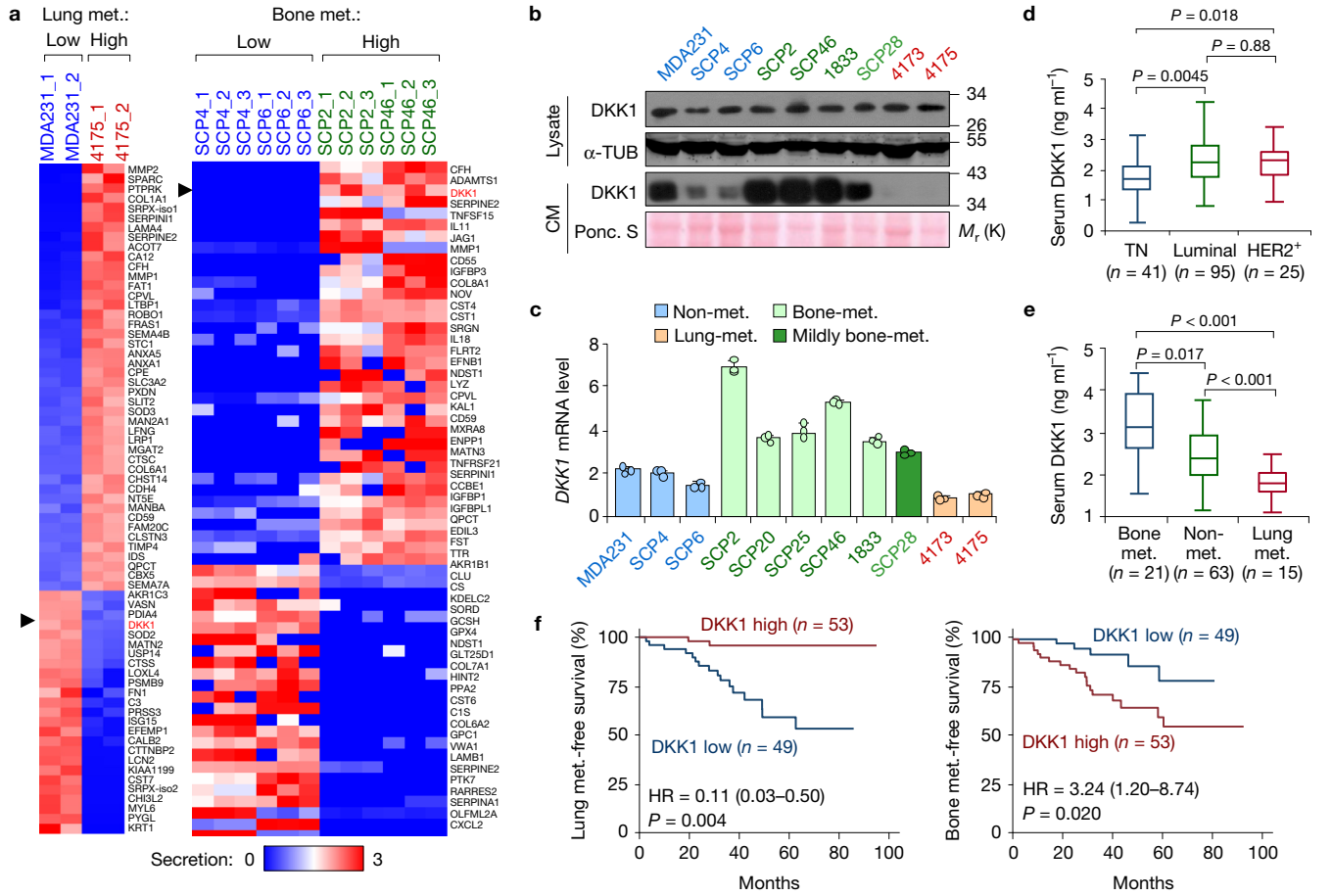

Figure 1 DKK1 secretion is associated with breast cancer metastasis organotropism. (**a**) Heatmap of mass-spectrum secretome analyses of MDA231 derivatives with different capabilities for lung and bone metastasis. The columns represent cell lines and the rows represent proteins. The arrowheads point to DKK1. (**b**,**c**) DKK1 protein (**b**) and *DKK1* mRNA (**c**, $n=3$ biologically independent samples) levels in MDA231 derivatives. Sky blue, light green, green and red fonts denote weakly metastatic, mildly bone-metastatic, highly bone-metastatic and highly lung-metastatic cell lines, respectively. CM, conditioned medium. (**d**) Serological DKK1 levels in the different breast cancer subtypes. (**e**) Serological DKK1 levels of Qilu breast cancer patients with different metastatic status. (**f**) Lung (left) and bone (right) metastasis-free survival analyses of Qilu patients according to serological DKK1 levels. *P* values were obtained by ANOVA followed by Holm's test (**d**,**e**) or log-rank test (**f**). Unprocessed original scans of blots are shown in Supplementary Fig. 9. Box plots display values of minimum, first quartile, median, third quartile, and maximum. Bar graphs are shown as mean ± s.d.

(MDA231) derivative cell lines with varied metastasis abilities to lungs and bone[2,17], and identified 69 and 59 extracellular proteins significantly regulated in lung- and bone-metastatic cells, respectively (Fig. 1a). Among the eight common proteins in the two lists (Supplementary Table 1), seven were upregulated in both metastasis organotropisms. However, one protein, DKK1, was obviously downregulated in lung metastasis but upregulated in bone metastasis (Fig. 1a). Further analyses confirmed the organotropic pattern of messenger RNA and extracellular protein levels of DKK1 in more MDA231 sublines (Fig. 1b,c). In addition, analysis of a Qilu cohort of breast cancer patients showed that serological DKK1 levels were significantly lower in triple-negative breast cancer (Fig. 1d), a subtype associated with higher risk of lung relapse[18]. Concordantly, DKK1 was downregulated in the patients with tumour recurrence only in the lungs, while upregulated in those with only bone recurrence, as compared with those without distant recurrence (Fig. 1e). Moreover, patients with less DKK1 in the serum were prone to lung metastasis, but were protected from bone metastasis (Fig. 1f). In contrast, other Dickkopf family member proteins were either undetectable in the patient sera (DKK2 and DKK4) or not correlated with metastasis (DKK3) (Supplementary Fig. 1a). These findings revealed a unique link between DKK1 and breast cancer organotropism.

DKK1 suppresses lung metastasis of breast cancer

To explore the biological function of DKK1 in lung metastasis, *DKK1* was stably overexpressed in a mildly metastatic breast cancer cell line SCP28 (ref. 2) (Supplementary Fig. 1b,c and Fig. 2a). *DKK1* overexpression significantly reduced lung-metastatic burden and extended animal survival (Fig. 2b–d). Noticeably, both early seeding of cancer cells (Supplementary Fig. 1d and Fig. 2e) and metastatic growth at the later stage (Supplementary Fig. 1e and Fig. 2f) were inhibited by *DKK1* overexpression. In contrast, *DKK1* knockdown by short hairpin RNAs (shRNAs) (Fig. 2a and Supplementary Fig. 1b) exacerbated lung colonization and shortened metastasis-free survival of the mice (Fig. 2g,h).

We also analysed the role of DKK1 for lung metastasis in immunocompetent mice by overexpressing murine *Dkk1* in 4T1 cells and the primary cancer cells derived from a spontaneous

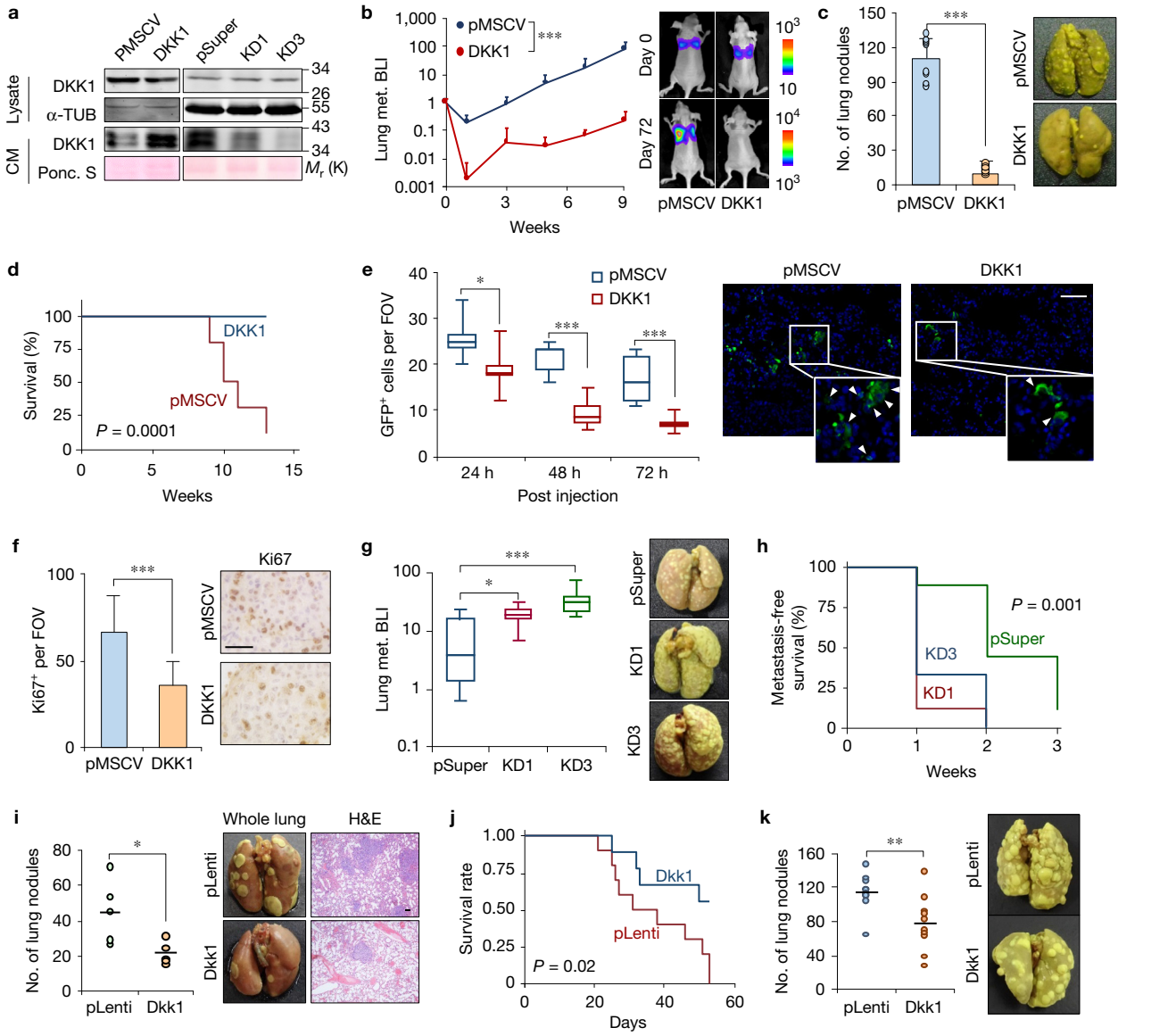

Figure 2 DKK1 inhibits lung metastasis of breast cancer. (**a**) *DKK1* overexpression and knockdown in SCP28 cells. (**b**–**f**) Intravenous injection of SCP28 cells with *DKK1* overexpression for lung colonization analysis ($n=10$ mice per group for **b**–**d**). Shown are bioluminescent imaging (BLI) quantification and images (**b**), pulmonary surface nodules (**c**), animal survival (**d**), GFP$^+$ cancer cell quantification in lung sections at the annotated time points (**e**, $n=12$ samples from 3 mice per group), and Ki67 staining of lung metastases (**f**, $n=21$ samples from 3 mice per group). (**g**,**h**) Intravenous injection of SCP28 cells with DKK1 knockdown (KD) for lung colonization analysis ($n=9$ mice per group). Shown are BLI quantification and whole-lung images (**g**), and metastasis-free survival of the mice (**h**). (**i**,**j**) Intravenous injection of 4T1 cells with murine *Dkk1* overexpression into BALB/c mice for lung metastasis ($n=10$ mice per group). Shown are pulmonary metastasis analyses (**i**) and survival rates (**j**) of the mice. H&E, haematoxylin and eosin. (**k**) Intravenous injection of PyMT primary cancer cells with *Dkk1* overexpression into C57BL/6J mice for lung metastasis ($n=10$ mice per group). Scale bars, 50 μm. $^*P<0.05$, $^{**}P<0.01$, $^{***}P<0.001$ by repeated measures ANOVA (**b**), log-rank test (**d**,**h**,**j**), ANOVA followed by Dunnett's test (**g**) or Student's *t*-test (all others). FOV, field of view. Unprocessed original scans of blots are shown in Supplementary Fig. 9. Box plots display values of minimum, first quartile, median, third quartile, and maximum. Bar graphs are shown as mean ± s.d.

tumour of MMTV-PyMT mice (Supplementary Fig. 1f). Again, *Dkk1* significantly suppressed lung metastasis and extended animal survival when 4T1 and PyMT cells were injected into syngeneic BALB/c or C57BL/6J mice (Fig. 2i–k).

DKK1 suppresses macrophage and neutrophil recruitment in lung metastases

To analyse the mechanism by which DKK1 regulates lung metastasis, we first assessed the effects of DKK1 on cancer cell intrinsic malignancy and found that *in vitro* cell growth, tumour sphere formation, apoptosis, migration and trans-endothelial invasion of cancer cells stayed unchanged after *DKK1* overexpression and knockdown (Supplementary Fig. 1g–k). Therefore, we focused on microenvironmental changes in lung metastases after *DKK1* manipulation.

Various stromal components, including macrophages, neutrophils, endothelial cells, fibroblasts, mesenchymal stem cells and natural killer cells, have been shown to play important roles in cancer metastasis to lungs[19–27]. We performed flow cytometry analyses of these

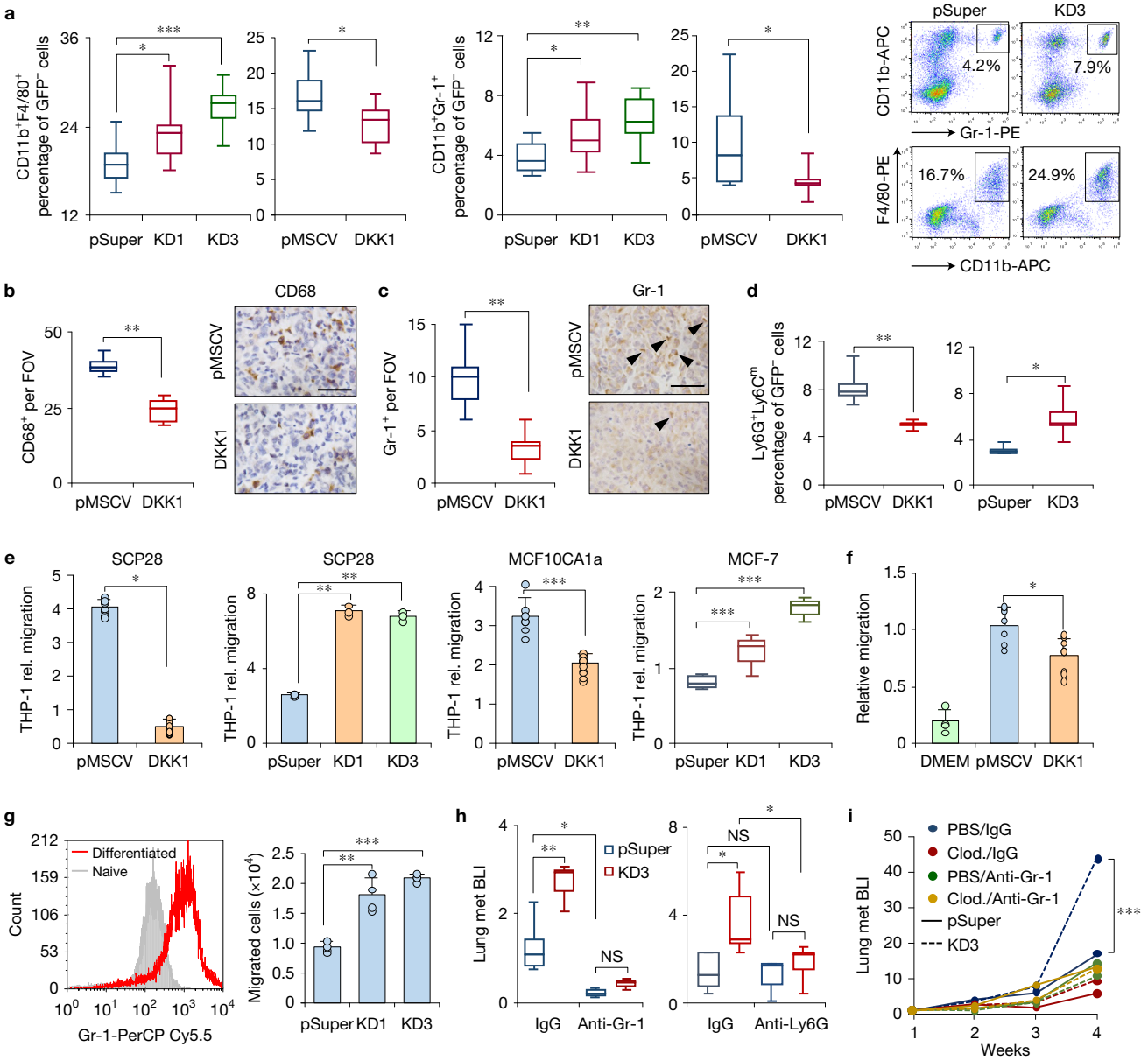

Figure 3 DKK1 attenuates macrophage and neutrophil recruitment in lung metastases. (**a**) Flow cytometry analysis of Gr-1$^+$ and F4/80$^+$ components in GFP$^-$ host cells of lung metastases by SCP28 (GFP$^+$) cells with *DKK1* knockdown or overexpression ($n=8$ biologically independent samples per group). Shown on the right are representative flow cytometry results. (**b**,**c**) IHC analyses of CD68$^+$ (**b**) or Gr-1$^+$ (**c**) cells in lung metastases by *DKK1*-overexpressing SCP28 ($n=10$ and 16 samples from 3 mice per group for **b** and **c**, respectively). The arrowheads point to Gr-1$^+$ cells. (**d**) CD11b$^+$Ly6G$^+$Ly6C^m cell contents in lung metastases with *DKK1* overexpression or knockdown ($n=5$ biologically independent samples per group). (**e**) Two-chamber migration assay of THP-1 cells recruited by CM from SCP28, MCF10CA1a or MCF7 cells, with *DKK1* overexpression or knockdown ($n=8$, 3, 7 and 8 biologically independent samples per group for each panel). (**f**,**g**) Two-chamber migration assay of bone-marrow-derived primary CD11b$^+$Gr-1$^+$ myeloid cells recruited by DMEM medium, or CM of control SCP28 cells or SCP28 cells with *DKK1* overexpression (**f**) or knockdown (**g**). $n=4$ biologically independent samples per group. The identity of myeloid cells is validated by Gr-1 flow cytometry (**g**, left panel). (**h**) BLI quantification of control and *DKK1* KD3 SCP28 lung metastasis treated with depletion antibodies against Gr-1 (RB6-8C5) or Ly6G (1A8) at 2 weeks post SCP28 injection ($n=5$ mice per group). (**i**) Lung metastasis by SCP28 *DKK1* KD3 or control cells treated with clodronate liposomes (PBS liposomes as the control) and the Gr-1$^+$ clearance antibody RB6-8C5 (IgG as the control). Line types indicate cell lines and colours of the lines/dots indicate treatment conditions ($n=5$ mice per group). Scale bars, 50 μm. $^*P<0.05$, $^{**}P<0.01$, $^{***}P<0.001$ by repeated measures ANOVA (**i**), ANOVA followed by Dunnett's (**a**,**e**,**g**) or Holm's test (**h**), or Student's *t*-test (all others). NS, not significant. Box plots display values of minimum, first quartile, median, third quartile, and maximum. Bar graphs are shown as mean ± s.d.

non-tumour cell populations in lung metastases (Supplementary Fig. 2a), and found that *DKK1* overexpression enhanced, while knockdown suppressed, the percentages of CD11b$^+$F4/80$^+$ macrophages and CD11b$^+$Gr-1$^+$ myeloid cells, but not other stromal components in lung metastases (Fig. 3a and Supplementary Fig. 2b), which was further confirmed by immunohistochemistry (IHC) analyses of the metastasis tissues (Fig. 3b,c). The changes of these immunocytes were not due to the alteration in their biogenesis, as their

abundance in the spleen or bone marrow of the mice stayed unchanged (Supplementary Fig. 2c).

The $CD11b^+Gr\text{-}1^+$ myeloid cells are a heterogeneous population of monocytes and neutrophils at various maturation stages, as the Gr-1 antibody recognizes both Ly6C and Ly6G antigens. Thus, we characterized the $CD11b^+Gr\text{-}1^+$ population with antibodies specific to Ly6C and Ly6G. The majority of the $CD11b^+$ cells in lung metastases were either $Ly6G^-Ly6C^-$ or $Ly6G^+Ly6C^m$, and few were $Ly6G^-Ly6C^{hi}$. In addition, most $CD11b^+Gr\text{-}1^+$ cells were also Ly6G positive (Supplementary Fig. 2d). The $CD11b^+Ly6G^+Ly6C^m$ cells, but not the $CD11b^+Ly6G^-Ly6C^{hi}$ cells, were obviously inhibited in lung metastases by *DKK1* expression (Fig. 3d and Supplementary Fig. 2e). The $CD11b^+Ly6G^+Ly6C^m$ cells expressed the granulocytic markers *Nos2* and *Prok2*, but not the monocytic marker *Arg1* (Supplementary Fig. 2f). These cells also displayed characteristic banded or segmented nuclei, as compared with the $CD11b^+Ly6G^-Ly6C^{hi}$ cells with the monocytic feature of large rounded nuclei (Supplementary Fig. 2g). These data suggested that the $CD11b^+Gr\text{-}1^+$ myeloid cells regulated by DKK1 were mainly $Ly6G^+$ neutrophils.

We further observed that *DKK1* overexpression suppressed the capability of cancer-cell-conditioned medium (CM) to attract THP-1 monocytes, without changing THP-1 proliferation (Fig. 3e and Supplementary Fig. 2h). In contrast, *DKK1* knockdown promoted CM-induced THP-1 migration (Supplementary Fig. 2i and Fig. 3e). The regulatory effect of DKK1 on immunocyte recruitment was also observed for primary macrophages and $CD11b^+Gr\text{-}1^+$ cells differentiated from murine bone marrow (Fig. 3f,g and Supplementary Fig. 2j).

In addition, when macrophages and neutrophils were depleted in the mice with clodronate liposomes and the anti-Gr-1 clearance antibody RB6-8C5 prior to cancer cell injection (Supplementary Fig. 2k,l), the promotion of metastatic seeding and colonization in lungs by *DKK1* knockdown was abolished (Fig. 3h,i and Supplementary Fig. 2m). Specific depletion of neutrophils with the Ly6G antibody (1A8) resulted in similar suppression of lung colonization (Supplementary Fig. 2k and Fig. 3h). Meanwhile, co-culturing SCP28 with macrophages resulted in macrophage dosage-dependent promotion of cancer cell growth (Supplementary Fig. 2n). These data were concordant with the observations that DKK1 suppressed both early seeding and metastatic growth of cancer cells in lungs (Supplementary Fig. 1d,e and Fig. 2e,f). Therefore, the suppressive function of DKK1 in lung metastasis was mediated by reduced immunocyte recruitment.

DKK1 suppresses immunocyte recruitment by inhibiting the JNK–PTGS2 signal axis of cancer cells

Next we interrogated the mechanism by which DKK1 affects macrophage and neutrophil recruitment. It was found that tumour-derived DKK1 played an autocrine role for immunocyte recruitment, as addition of recombinant DKK1 proteins into cancer cell culture prior to CM collection, but not that directly into CM, phenocopied *DKK1* overexpression and significantly impaired CM-induced THP-1 migration (Fig. 4a).

We also found that immunocyte suppression by DKK1 was probably due to inhibition of non-canonical, but not canonical, WNT signalling. First, expressing the dominant-negative mutants of LEF1 (ΔC-LEF1) or TCF4 (ΔN-TCF4) in SCP28 (Supplementary Fig. 3a–d) to inhibit canonical WNT signalling did not suppress lung metastasis, and could not rescue the effect of *DKK1* knockdown for immunocyte recruitment (Fig. 4b,c and Supplementary Fig. 3e–h). Notably, ΔC-LEF1 rather enhanced lung metastasis, a phenomenon probably due to an indirect effect of ΔC-LEF1 to suppress the expression of *DKK1* (Supplementary Fig. 3a), which is also a downstream target of canonical WNT signalling[28]. Second, expressing the constitutively active β-catenin (ΔN-CTNNB1) (Supplementary Fig. 3a,b,d) also failed to rescue the suppressing effect of *DKK1* overexpression in lung metastases (Fig. 4b,d and Supplementary Fig. 3g). Third, expressing the typical non-canonical WNT ligand WNT5A (Supplementary Fig. 3i) phenocopied *DKK1* knockdown and opposed the effect of *DKK1* overexpression in THP-1 recruitment (Fig. 4e–g and Supplementary Fig. 3j,k). Fourth, other soluble WNT inhibitors *DKK2/3/4* and *SFRP2* did not obviously regulate THP-1 migration, although they inhibited β-catenin (Supplementary Fig. 3l,m).

Then we assessed which non-canonical WNT signalling pathways were regulated by DKK1 in breast cancer cells. Among the possible non-canonical WNT/PCP and WNT/Ca^{2+} downstream signalling pathways, downregulation of the RAC1–JNK–JUN axis, which is downstream of the PCP signalling[6], and the CaMKII–NF-κB axis, which is downstream of the Ca^{2+} signalling[5], were observed after *DKK1* overexpression in multiple cancer cell lines (Fig. 4h and Supplementary Fig. 4a). Concordantly, *DKK1* knockdown activated these two signalling axes (Supplementary Fig. 4b). Other reported non-canonical WNT downstream pathways, including Rho, PKC, ERK, AKT, p38 and NFAT[5,6], were not affected by DKK1 (Supplementary Fig. 4c–e). Furthermore, *JUN* overexpression or treating cancer cells with RAC1 and JNK inhibitors (EHop-016, SP600125), but not inhibitors of Ca^{2+} signalling or other WNT downstream pathways, regulated CM-induced THP-1 recruitment (Fig. 4i–k). However, direct treatment of THP-1 with SP600125 was not able to suppress THP-1 migration induced by cancer cell CM (Supplementary Fig. 4f).

The above data indicated that DKK1 might regulate some tumour-secreted factors involved in immunocyte recruitment by inhibiting WNT/PCP–JNK signalling. To search for such factors, we compared the control and *DKK1*-overexpressing SCP28 cells by mass-spectrum secretome profiling, which identified ten proteins with a consistent difference among three biological replicates (Supplementary Table 2), and quantitative PCR (qPCR) screening of an *ad hoc* list (Supplementary Table 3) of immunocyte migration-related genes manually curated from previous publications[29,30], which identified PTGS2 (also known as COX2). PTGS2, the rate-limiting catalyser for production of hormone-like prostaglandin E2 (PGE_2), was a promising candidate as PGE_2 has been shown to potently regulate immunocyte recruitment[31]. We confirmed that *PTGS2* expression, as well as the extracellular PGE_2 level, of cancer cells was modulated coordinately by *DKK1*, *WNT5A* and the JNK inhibitor, but not the CaMKII inhibitor in various cancer cell lines (Fig. 5a,b and Supplementary Figs 3i and 4a,g,h). Chromatin immunoprecipitation (ChIP)-qPCR assays revealed approximately tenfold enrichment of JUN occupancy on multiple sites of the *PTGS2* promoter (Fig. 5c), indicating that PTGS2 is a direct transcriptional target of JUN.

To verify the role of PTGS2 in immunocyte recruitment, cancer cells were treated with the PTGS2 inhibitor celecoxib and a reduction of THP-1 migration induced by cancer cell CM was observed (Fig. 5d). Moreover, *PTGS2* overexpression in SCP28 was able to

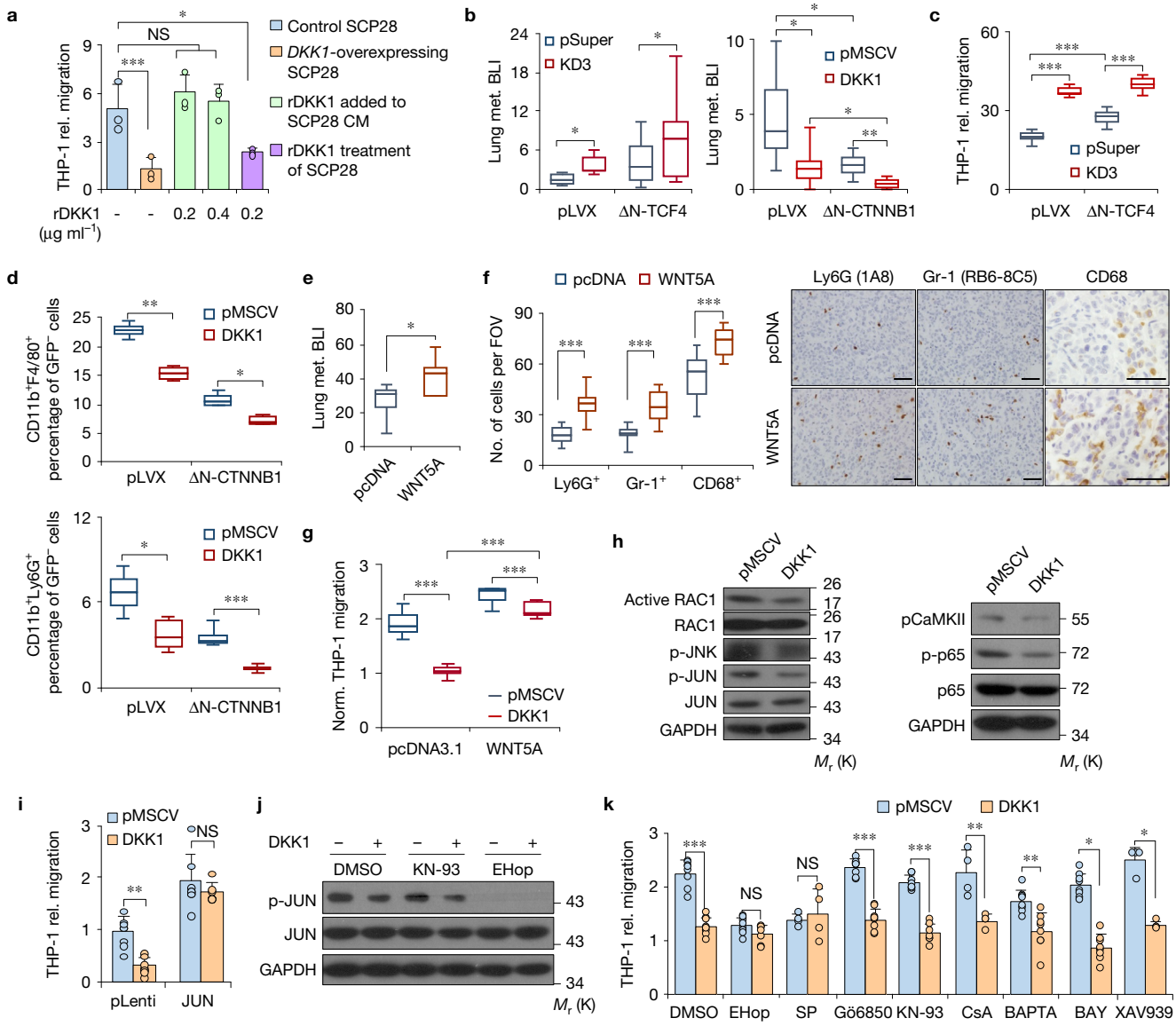

Figure 4 DKK1 attenuates immunocyte recruitment by regulating RAC1–JNK signalling. (**a**) The effects of *DKK1* overexpression, recombinant DKK1 treatment of cancer cells or cancer cell CM on CM-induced THP-1 recruitment ($n=3$ biologically independent samples per group). (**b**) SCP28 lung metastasis with *DKK1* knockdown and ΔN-TCF4 (left), or *DKK1* overexpression and ΔN-CTNNB1 (right). $n=8$ mice per group. (**c**) THP-1 migration induced by CM of SCP28 cells with *DKK1* knockdown and ΔN-TCF4 ($n=8$ biologically independent samples per group). (**d**) Macrophage (top) and neutrophil (bottom) contents in lung metastases by SCP28 cells with *DKK1* overexpression and ΔN-CTNNB1 ($n=5$ biologically independent samples per group). (**e**–**g**) The effects of *WNT5A* overexpression in SCP28 cells on lung metastasis (**e**, $n=6$ mice per group), Ly6G$^+$, Gr-1$^+$ and CD68$^+$ cell contents (**f**, $n=10$ samples from 3 mice per group) in lung metastases, and CM-induced THP-1 migration (**g**, $n=8$ biologically independent samples per group). Scale bars, 50 μm. (**h**) The effect of DKK1 on the RAC1–JNK–JUN (left) and CaMKII–NF-κB (right) pathways in SCP28. (**i**) THP-1 recruitment by CM of SCP28 cells with *DKK1* and *JUN* overexpression ($n=8$ biologically independent samples per group). (**j**) JUN phosphorylation in SCP28 is suppressed by the RAC1 inhibitor EHop, but not the CaMKII inhibitor (KN-93). (**k**) THP-1 recruitment by CM of SCP28 cells with or without *DKK1* overexpression, and pre-treated with inhibitors of various pathways, including RAC1 (EHop-016, EHop), JNK (SP600125, SP), PKC (Gö6850), CaMKII (KN-93), calcineurin/NFAT (cyclosporin A, CsA), calcium (BAPTA), NF-κB (BAY11-7082, BAY) and canonical WNT (XAV939). $n=4$ (SP, CsA and XAV), 7 (EHop and KN-93) or 8 (all others) biologically independent samples per group. $^*P<0.05$, $^{**}P<0.01$, $^{***}P<0.001$ by ANOVA followed by Dunnett's (**a**) or Holm's test (**b**,**c**,**g**), or Student's *t*-test (all others). NS, not significant. Unprocessed original scans of blots are shown in Supplementary Fig. 9. Box plots display values of minimum, first quartile, median, third quartile, and maximum. Bar graphs are shown as mean ± s.d.

abolish the suppressive effect of *DKK1* and SP600125 on THP-1 migration (Fig. 5e). Reciprocally, *PTGS2* knockdown in SCP28 suppressed *DKK1*-knockdown-induced THP-1 migration (Fig. 5f). In addition, supplying cancer cell CM with PGE_2 enhanced macrophage and neutrophil migration, and diminished the effects of *DKK1* and SP600125 (Fig. 5g,h and Supplementary Fig. 4i). Concordantly, the PGE_2 receptors *PTGER2* and *PTGER4* were highly expressed in THP-1, macrophages and primary CD11b$^+$Gr-1$^+$ myeloid cells, but not in cancer cells or other stromal cells (Supplementary Fig. 4j). Collectively, these data suggested that DKK1 attenuated immunocyte recruitment by inhibiting WNT/PCP–JNK signalling and *PTGS2* expression.

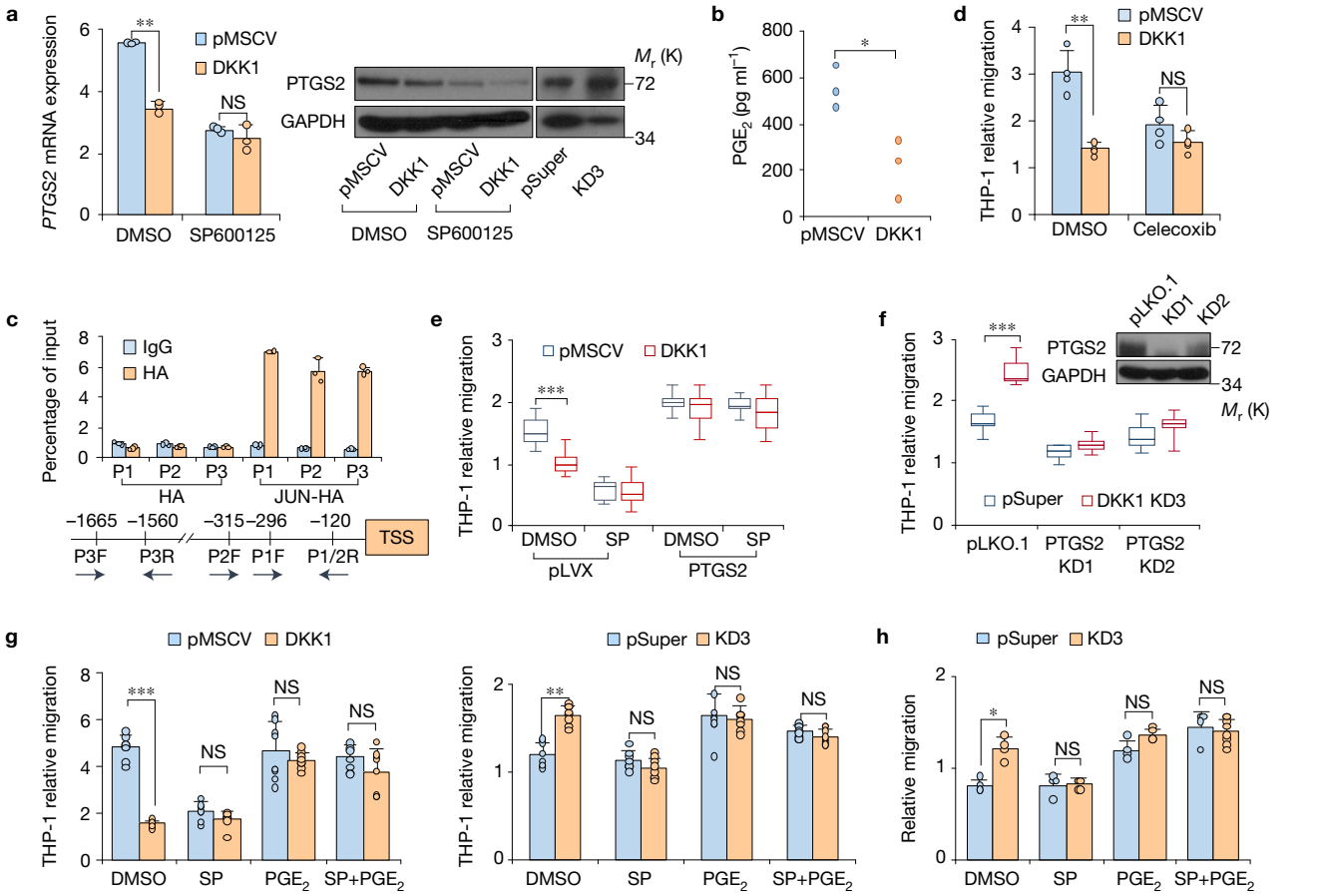

Figure 5 DKK1 suppresses PTGS2 by regulating the RAC1–JNK pathway. (**a**) *PTGS2* mRNA and protein levels in SCP28 cells after *DKK1* overexpression and knockdown, and treatment with the JNK inhibitor SP600125. $n=3$ biologically independent samples per group. (**b**) PGE_2 levels in SCP28 CM after *DKK1* overexpression. $n=3$ biologically independent samples per group. (**c**) ChIP–qPCR analysis of JUN binding on the *PTGS2* promoter ($n=3$ biologically independent samples per group). The lower panel shows the position of the qPCR primers on the promoter. (**d**) THP-1 recruitment by CM of control or *DKK1*-overexpressing SCP28 cells treated with the PTGS2 inhibitor celecoxib ($n=4$ biologically independent samples per group). (**e**) THP-1 migration induced by CM from SCP28 cells with *DKK1* and *PTGS2* overexpression and SP600125 treatment ($n=12$ biologically independent samples per group). (**f**) THP-1 migration induced by CM from SCP28 cells with *DKK1* overexpression and *PTGS2* knockdown ($n=8$ biologically independent samples per group). Inset, validation of *PTGS2* knockdown. (**g**,**h**) THP-1 (**g**) and primary Gr-1^+ myeloid cell (**h**) recruitment by CM of SP600125-pre-treated SCP28 cells. PGE_2 was added directly into the CM ($n=8$ and 4 biologically independent samples per group for **g** and **h**, respectively). $^*P<0.05$, $^{**}P<0.01$, $^{***}P<0.001$; NS, not significant, by Student's *t*-test. Unprocessed original scans of blots are shown in Supplementary Fig. 9. Box plots display values of minimum, first quartile, median, third quartile, and maximum. Bar graphs are shown as mean ± s.d.

DKK1 suppresses cancer cell LTBP1 and TGF-β1 secretion via CaMKII–NF-κB signalling

Among the secretory proteins identified by mass-spectrum analysis (Supplementary Table 2), latent TGF-β-binding protein 1 (LTBP1) was also noteworthy as both our data (Fig. 1a) and previous studies[1] showed that it was upregulated in lung-metastatic cancer cells. LTBP1 is known to bind to the latent form of TGF-β and escort its secretion, thus enhancing TGF-β bioavailability[32]. Given the important role of TGF-β signalling for breast-to-lung metastasis[24,33], we sought to assess the involvement of LTBP1 in DKK1 regulation of lung metastasis.

First we found that LTBP1 was highly expressed in the lung-tropic lines as compared with other MDA231 derivatives (Fig. 6a). *DKK1* overexpression reduced LTBP1 expression and secretion (Fig. 6a and Supplementary Fig. 5a,b), while *DKK1* knockdown and *WNT5A* overexpression resulted in LTBP1 upregulation (Fig. 6b and Supplementary Fig. 3i). In addition, knocking down LTBP1 with shRNAs led to a decrease in TGF-β1 secretion (Fig. 6c). Concordantly, DKK1 reduced the secretion, but not the mRNA level, of TGF-β1 in SCP28 (Fig. 6d and Supplementary Fig. 5c). When SCP28 CM was heated to activate latent TGF-β (ref. 34), a suppressive effect of DKK1 on CM-elicited TGF-β responses, as shown by SMAD-binding element (SBE) reporter activity and SMAD2 phosphorylation (Supplementary Fig. 5d and Fig. 6e), and SCP28 invasiveness (Fig. 6f), were observed. These data indicated that DKK1 suppressed LTBP1 expression and TGF-β bioavailability in cancer cell CM.

Then we sought to delineate the molecular pathway by which DKK1 inhibits LTBP1. Inhibition of CaMKII–NF-κB, but not RAC1–JNK, drastically suppressed the extracellular LTBP1 level and enhanced the effect of *DKK1* overexpression on LTBP1 regulation in SCP28 and MCF10CA1a (Fig. 6a and Supplementary Fig. 5e-g). LTBP1 expression was also regulated by the NF-κB transcription factor RELA and the super inhibitor IκBαM (Supplementary Fig. 5h). In addition, we confirmed DKK1 regulation of NF-κB signalling with analyses of NF-κB-responsive reporter and p65 nuclear localization

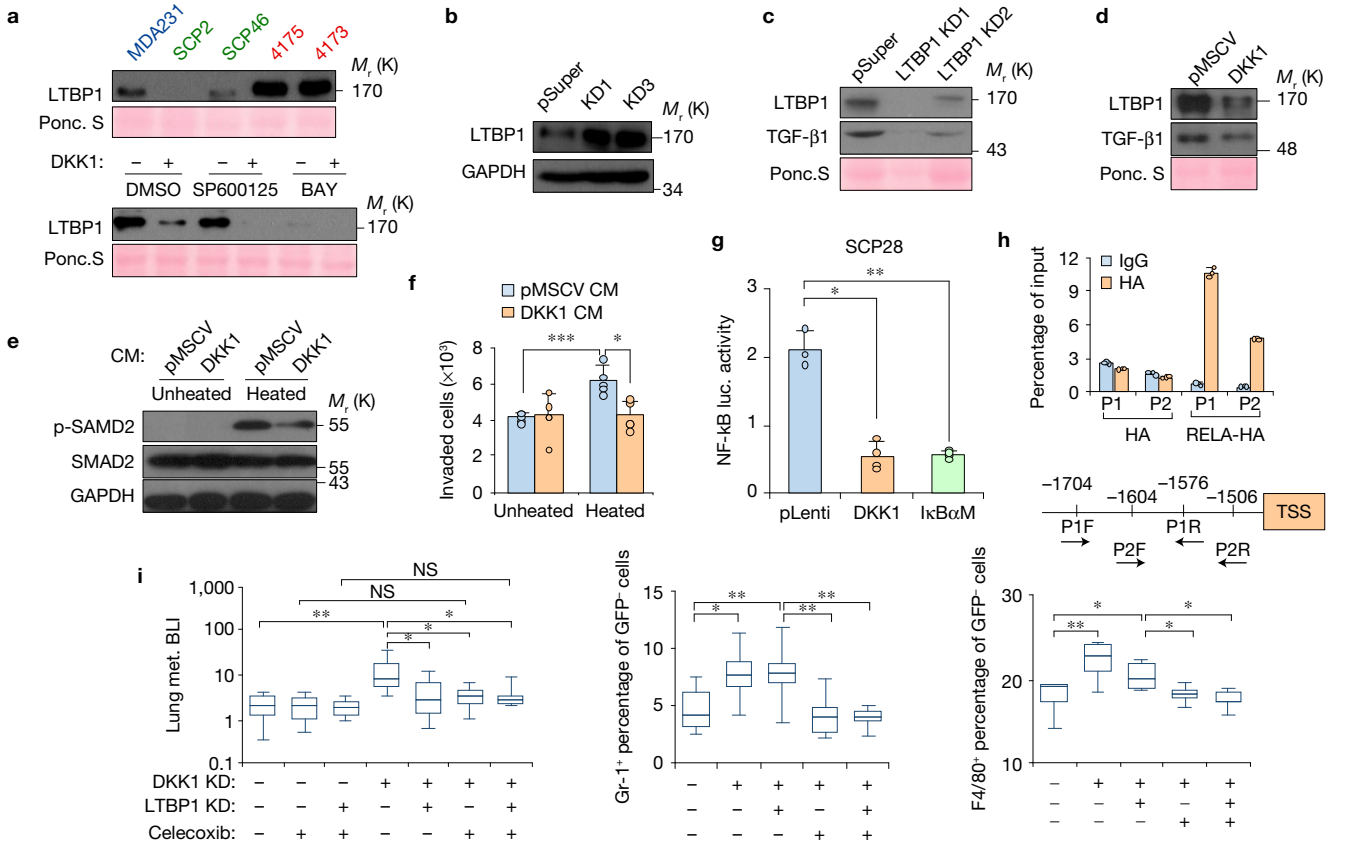

Figure 6 DKK1 suppresses LTBP1 via NF-κB signalling. (**a**) LTBP1 secretion in MDA231 derivatives (top) and in SCP28 treated with JNK (SP600125) and NF-κB (BAY11-7082) inhibitors (bottom). (**b**) LTBP1 expression in SCP28 cells after *DKK1* knockdown. (**c**) LTBP1 and TGF-β1 secretion level in SCP28 cells after *LTBP1* knockdown. (**d**) TGF-β1 secretion in SCP28 after *DKK1* overexpression. (**e**) SMAD2 phosphorylation in HeLa cells treated with CM from *DKK1*-overexpressing SCP28 cells, with or without heating activation of latent TGF-β1 in the CM. (**f**) Invasiveness of SCP28 cells treated with CM from *DKK1*-overexpressing SCP28 cells, with or without heating ($n=5$ biologically independent samples per group). (**g**) NF-κB-responsive reporter activity in SCP28 cells transfected with *DKK1* or IκBαM ($n=4$ biologically independent samples per group). (**h**) ChIP–qPCR analysis of RELA binding on the *LTBP1* promoter ($n=3$ biologically independent samples per group). The alignment positions of the qPCR primers on the LTBP1 promoter are shown in the lower panel. (**i**) Lung-metastasis BLI (left, $n=10$ mice per group) and Gr-1$^+$ (middle, $n=6$ biologically independent samples per group) or F4/80$^+$ (right, $n=6$ biologically independent samples per group) cell percentages in mice with intravenous injection of SCP28 cells with *DKK1* or *LTBP1* knockdown, and treated with celecoxib. $^*P<0.05$, $^{**}P<0.01$, $^{***}P<0.001$ by ANOVA followed by Dunnett's (**f**,**g**) or Holm's test (**i**), or Student's *t*-test (all others). NS, not significant. Unprocessed original scans of blots are shown in Supplementary Fig. 9. Box plots display values of minimum, first quartile, median, third quartile, and maximum. Bar graphs are shown as mean ± s.d.

(Fig. 6g and Supplementary Fig. 5i,j). Further, deletion of the consensus NF-κB-binding site in the LTBP1 promoter markedly reduced the promoter activity and diminished its response to NF-κB inhibitors (Supplementary Fig. 5k,l). More directly, ChIP–qPCR analysis showed RELA occupancy around the NF-κB-binding site (Fig. 6h). These data indicated that DKK1 suppressed LTBP1 expression by regulating the WNT/Ca^{2+}–CaMKII–NF-κB axis.

PTGS2 and LTBP1 mediate the effect of DKK1 in lung metastasis

LTBP1 knockdown (Fig. 6c) and mouse treatment by celecoxib effectively blocked the advantage of *DKK1*-silenced cells for lung colonization (Fig. 6i). Notably, celecoxib treatment, but not *LTBP1* knockdown, reduced Gr-1$^+$ and macrophage percentages in lung metastases (Fig. 6i), which was concordant with the observation that LTBP1 did not regulate *in vitro* immunocyte migration (Supplementary Fig. 6a). In addition, *LTBP1* knockdown reversed the enhancement of SMAD3 phosphorylation in lung metastases caused by *DKK1* silencing (Supplementary Fig. 6b). These data corroborated our conclusion that PTGS2 and LTBP1 regulate immunocyte recruitment and TGF-β bioavailability, respectively, during lung colonization.

Further, we assessed the correlation of PTGS2 and LTBP1 with breast cancer metastasis organotropism. In the MDA231 derivative cells, both *PTGS2* and *LTBP1* expression positively correlated with cellular capabilities of lung metastasis, but not bone metastasis (Supplementary Fig. 6c). In the Qilu clinical cohort, serological DKK1 levels were inversely correlated with PGE_2 levels (Supplementary Fig. 6d). IHC analyses also revealed an inverse correlation of DKK1 with LTBP1 and PTGS2 in tumour samples (Supplementary Fig. 6e). Altogether, these data suggested that LTBP1 and PTGS2 mediate the role of DKK1 for lung metastasis of breast cancer.

The dichotomous role of DKK1 in metastasis organotropism

In contrast to the suppressive role of DKK1 in breast cancer lung metastasis, previously studies have shown that DKK1 promotes breast cancer bone metastasis by regulating osteoclastogenesis[13–16]. To check

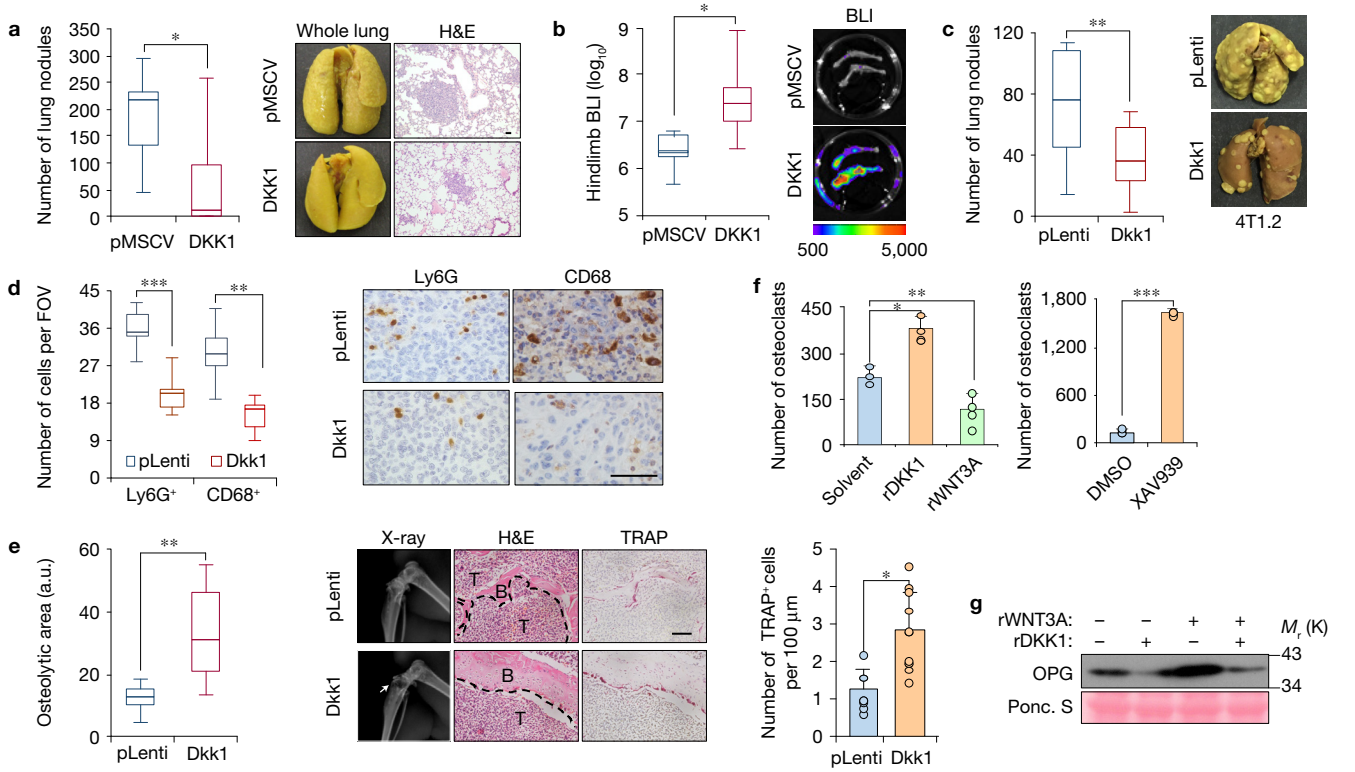

Figure 7 The dichotomous role of DKK1 in breast cancer metastasis organotropism. (**a**,**b**) Orthotopic injection of SCP28 cells with *DKK1* overexpression in NOD/SCID mice ($n=10$ mice per group). Shown are pulmonary metastasis nodules and H&E staining of lung sections (**a**), and *ex vivo* BLI quantification of hind legs (**b**) of the animals. (**c**–**e**) Orthotopic injection of 4T1.2 cells with *Dkk1* overexpression in BALB/c mice ($n=8$ mice per group in **a**–**c**). Shown are pulmonary metastasis nodules (**c**), Ly6G$^+$ and CD68$^+$ cells in lung metastases (**d**, $n=9$, 9, 11 and 6 biologically independent samples for each group), and osteolytic metastasis areas (**e**, $n=8$ mice for osteolytic area analysis and $n=7$ and 10 biologically independent samples for TRAP$^+$ analysis). In **e**, the arrow points to an osteolytic area in the leg. TRAP, tartrate-resistant acid phosphatase staining for mature osteoclasts; B, bone; T, tumour. (**f**) Osteoclastogenesis of primary bone marrow cells treated with solvent control, recombinant human DKK1 or WNT3A, or the canonical WNT inhibitor XAV939 ($n=4$ biologically independent samples per group). (**g**) Extracellular levels of OPG in MC3T3 cells treated with recombinant human DKK1 and/or WNT3A. Scale bars, 50 μm. $^*P<0.05$, $^{**}P<0.01$, $^{***}P<0.001$ by ANOVA followed by Dunnett's test (**f**) or Student's *t*-test (others). a.u., arbitrary unit. Unprocessed original scans of blots are shown in Supplementary Fig. 9. Box plots display values of minimum, first quartile, median, third quartile, and maximum. Bar graphs are shown as mean ± s.d.

whether DKK1 indeed plays a dichotomous role in metastasis organotropism, we first analysed the effect of DKK1 in bone metastasis by intracardiac injection of SCP28 into athymic mice. *DKK1* overexpression in SCP28 significantly increased bone metastasis and osteolysis, with upregulated tumour proliferation in metastases (Supplementary Fig. 7a), while *DKK1* knockdown decreased bone metastasis and alleviated animal paralysis (Supplementary Fig. 7b). These phenotypes were in sharp contrast to the effects of DKK1 in lung metastasis.

To further investigate the role of DKK1 in the whole multi-step metastasis process, we orthotopically grafted SCP28 cells into the mammary fat pads of NOD/SCID mice. Primary tumour growth was not obviously affected by *DKK1* overexpression (Supplementary Fig. 7c). However, *DKK1* significantly inhibited lung metastasis (Fig. 7a), but also led to a tenfold increase of bone metastasis in the same mice (Fig. 7b). *Dkk1* overexpression in 4T1.2 (Supplementary Fig. 7d), a cell line capable of spontaneous metastasis to both bone and lungs[35], also inhibited lung metastasis and immunocyte infiltration, but exacerbated bone metastasis at the same time following orthotopic transplantation of 4T1.2 into immunocompetent BALB/c mice (Fig. 7c–e), without significantly affecting primary tumour growth and cancer cell dissemination (Supplementary Fig. 7d,e). Thus, tumour-derived DKK1 plays an organ-specific, dichotomous role in breast cancer metastasis.

Consistent with previous reports[13–16], we observed that DKK1 led to an increase of osteoclasts along the tumour/bone interface of bone metastases (Fig. 7e and Supplementary Fig. 7a), and promoted osteoclastogenesis from primary bone marrow induced by cancer cell CM (Supplementary Fig. 7f,g), which is critical for osteolytic bone metastasis. In addition, adding recombinant DKK1 proteins and the canonical WNT inhibitor XAV939 into bone marrow culture enhanced osteoclastogenesis, while recombinant WNT3A, the canonical WNT ligand, opposed the pro-osteoclast effect (Fig. 7f). Osteoclast maturation is regulated by osteoblast-derived RANKL and its antagonist OPG[36]. Concordantly, DKK1 suppressed, while WNT3A enhanced, OPG expression and secretion of pre-osteoblast cells (Fig. 7g and Supplementary Fig. 7h). Therefore, DKK1 promotes osteoclastogenesis by regulating canonical WNT signalling of osteoblasts for bone metastasis.

Combinatory targeting of JNK and TGF-β signalling prevents metastasis to both organs

Canonical WNT targeting has long been the focus of efforts for anti-cancer drug development[12]. However, our data indicated that

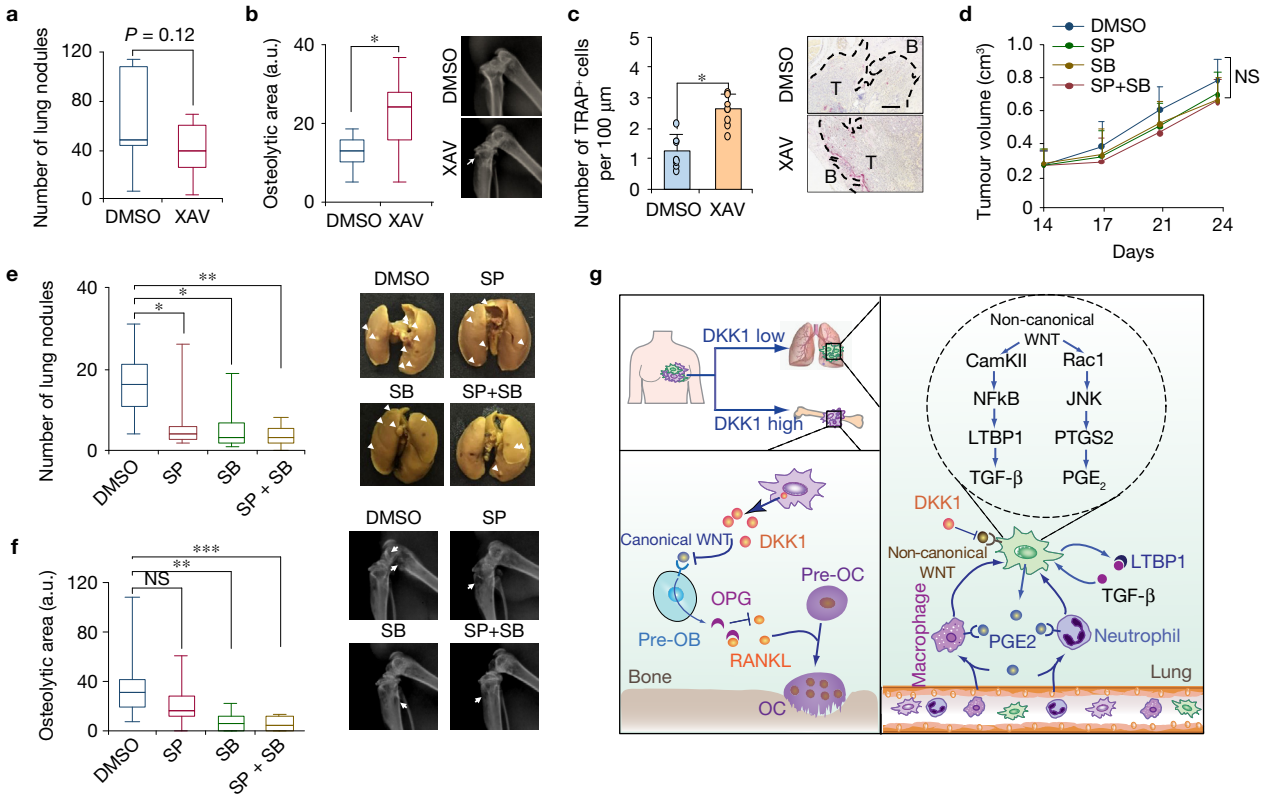

Figure 8 Therapeutic potentials of combinatory targeting of the JNK–PTGS2 and LTBP1–TGF-β pathways. (**a**–**c**) BALB/c mice with orthotopic 4T1.2 implantation were treated with XAV939 ($n=8$ mice per group for **a**,**b**) from day 14 post tumour implantation until euthanization. Shown are pulmonary tumour nodules (**a**), osteolytic lesions (**b**) and osteoclasts along the interface of bone metastases and bone (**c**, $n=7$ and 8 biologically independent samples per group). In **b**, the arrow points to an overt osteolytic lesion. B, bone; T, tumour. (**d**–**f**) BALB/c mice with orthotopic 4T1.2 implantation were treated with SP600125 (SP), SB431542 (SB) or both ($n=10$ mice per group) from day 14 post tumour implantation until euthanization. Shown are primary tumour growth (**d**), lung metastasis (**e**) and bone metastasis (**f**). The arrows and arrowheads in **e** and **f** point to lung surface nodules and overt bone lesions. (**g**) A schematic model of the dichotomous role of DKK1 in breast cancer metastasis. Scale bar, 50 µm. $^{*}P<0.05$, $^{**}P<0.01$, $^{***}P<0.001$; NS, not significant, by repeated measures ANOVA (**d**), ANOVA followed by Dunnett's test (**e**,**f**) or Student's *t*-test (others). Box plots display values of minimum, first quartile, median, third quartile, and maximum. Bar graphs are shown as mean ± s.d.

canonical WNT inhibition might not be optimal for metastatic cancer. Indeed, treating the BALB/c mice orthotopically grafted with 4T1.2 cells with the canonical WNT inhibitor XAV939 (Supplementary Fig. 8a) only marginally or insignificantly reduced primary tumour growth, cancer cell dissemination and lung metastasis (Fig. 8a and Supplementary Fig. 8b,c), but obviously exacerbated bone metastasis (Fig. 8b,c), demonstrating the lack of efficacy to stop lung metastasis and the deleterious effect on bone metastasis by the canonical WNT-targeting strategy.

Alternatively, we tested the effects of individual and combinatory targeting of DKK1-regulated downstream signalling with the JNK inhibitor SP600125 and the TGF-βRI inhibitor SB431542 in mice bearing 4T1.2 primary tumours (Supplementary Fig. 8d). All treatments had very modest effects on primary tumour growth (Fig. 8d), but significantly alleviated lung metastasis (Fig. 8e). In addition, TGF-β inhibition and the combinatory therapy also obviously suppressed osteolytic metastasis (Fig. 8f), consistent with the known role of TGF-β signalling in osteolysis[15] and our observation that SB431542, but not SP600125, was able to suppress osteoclastogenesis *in vitro* (Supplementary Fig. 8e). Importantly, the combinatory therapy was effective in suppressing metastasis to both organs, thus representing a rational strategy to treat metastasis.

DISCUSSION

Previous studies have identified a plethora of genes manipulating organ-specific metastasis. However, genes with different or contradictory roles in metastasis to multiple organs are rarely reported. DKK1 represents such a Janus-faced molecule in breast cancer metastasis (Fig. 8g). The role of DKK1 in cancer metastasis relies on the target organs, emphasizing the microenvironment dependence of metastasis regulatory molecules. Interestingly, although the TGF-β signalling pathway is also of great importance for osteolytic metastasis[15], downregulation of LTBP1 and TGF-β1 secretion by *DKK1* overexpression did not interfere with bone metastasis. The apparent inconsistency could be attributed to the rich reservoir of TGF-β in bone matrix[37], and thus reduced TGF-β secretion by *DKK1*-expressing tumour cells may be easily compensated by TGF-β release following osteolysis. Alternatively, the different outcomes of DKK1 in bone and lungs could be attributed to potential functional partners of DKK1 that are differentially present in various organs.

Several precautions should be taken to interpret our data regarding DKK1-regulated immunocytes during lung metastasis. First, the $CD11b^{+}Gr\text{-}1^{+}Ly6G^{+}Ly6C^{m}$ neutrophils are also referred to as the granulocytic subset of myeloid-derived suppressor cells in some studies due to their suppressive effect on T cells[27,38]. However, such

an immunosuppressive role of neutrophils was unlikely pertinent in the assays with immunodeficient mice. Notably, neutrophils could affect metastatic colonization by a number of mechanisms other than immunosuppression[27]. Second, although our data showed the roles of neutrophils and macrophages to promote early seeding and outgrowth of lung metastases, respectively, which is consistent with several previous studies[19–22], the effects of these immunocytes in other metastatic steps could not be ruled out. Third, the Gr-1 antibody that could target both neutrophils and monocytes appeared to be more potent in metastasis suppression than the neutrophil-depleting Ly6G antibody (Fig. 3h), suggesting the involvement of an admixture of immunocytes, including macrophages, neutrophils and monocytes in lung metastases.

In breast cancer patients, high and low serological DKK1 levels are associated with risk of bone and lung recurrence, respectively. Interestingly, other Dickkopf family members do not share the role of DKK1 in breast cancer lung and bone metastasis, which may not be surprising as previous studies have indicated the functional differences of DKK siblings[39–45]. The unique secretory pattern of DKK1 in organ-specific metastasis bestows it with the prognostic potential to predict metastasis organotropism. However, the detailed mechanism of how DKK1 regulates non-canonical WNT, such as its proximal ligands or receptors in the pathway, is yet to be delineated. Furthermore, its role in cancer could also be further studied in spontaneous tumour models of genetically engineered mice.

Importantly, our study emphasizes that caution should be taken to target WNT signalling in cancer, as such treatment may result in symptom complication, especially for those prone to bone metastasis. The outcome of canonical WNT targeting in lung metastasis might be even worse as WNT inhibition could also render the disseminated cancer cells resistant to immune clearance at the early stage of metastasis[26]. Alternatively, targeting the pathways downstream of non-canonical WNT signalling could be more effective to stop metastasis of multiple organs. Targeting TGF-β alone also showed dual efficiency to interfere with metastasis in both organs, but the combinatory approach displays modest enhancement for treatment of lung metastasis, in terms of lower variation among animals. Thus, our data provide a rationale for the combinatory JNK- and TGF-β-targeting strategy to treat metastatic diseases.

Overall, our data indicate that cancer metastasis should be regarded and treated as a systemic disease. In late-stage patients, the affected organs will not be confined. Mere emphasis on selected target organs in research and therapy is not sufficient or is even perilous for patients. Thus, either precise stratification of patients for metastasis organotropism or systemic scrutiny of potential intervention approaches should be performed to ensure therapeutic efficacy and safety. □

METHODS

Methods, including statements of data availability and any associated accession codes and references, are available in the online version of this paper.

Note: Supplementary Information is available in the online version of the paper

ACKNOWLEDGEMENTS

We thank L. Li at SIBS for providing the TOP/FOPFLASH, ΔN-CTNNB1 and ΔC-LEF1 constructs; D. Xie at SIBS for providing the ΔN-TCF4 construct; Y. Xiao at SIBS for providing the RELA construct; M. Liu at SIBS for providing the PTGS2 construct; and X. Miao, H. Zhang, S Yan and P. Zhou at the Institute of Health Sciences core facilities for technical support. G.H. was funded by the National Natural Science Foundation of China (81430070, 81661148048, 31371409), the Chinese Academy of Sciences (QYZDB-SSW-SMC013, XDA12050101), the Ministry of Science and Technology of China (2013CB910904) and the Science and Technology Commission of Shanghai Municipality (14431900800).

AUTHOR CONTRIBUTIONS

G.H. supervised the work. X.Zhuang and G.H. designed the experiments and drafted the manuscript. X.Zhuang, H.Z., M.C., F.P., J.Y. and X.Zhang performed the experiments. X.L. and Q.Y. contributed in clinical sample collection and analysis. Q.Y. helped design the experiments. All authors discussed the results and commented on the manuscript.

COMPETING FINANCIAL INTERESTS

The authors declare no competing financial interests.

Published online at http://dx.doi.org/10.1038/ncb3613

1. Minn, A. J. *et al.* Genes that mediate breast cancer metastasis to lung. *Nature* **436,** 518–524 (2005).
2. Kang, Y. *et al.* A multigenic program mediating breast cancer metastasis to bone. *Cancer Cell* **3,** 537–549 (2003).
3. Bos, P. D. *et al.* Genes that mediate breast cancer metastasis to the brain. *Nature* **459,** 1005–1009 (2009).
4. Michigami, T. *et al.* The effect of the bisphosphonate ibandronate on breast cancer metastasis to visceral organs. *Breast Cancer Res. Treat.* **75,** 249–258 (2002).
5. De, A. Wnt/Ca2+ signaling pathway: a brief overview. *Acta Biochim. Biophys. Sin (Shanghai)* **43,** 745–756 (2011).
6. Gao, C. & Chen, Y. G. Dishevelled: the hub of Wnt signaling. *Cell Signal.* **22,** 717–727 (2010).
7. Glinka, A. *et al.* Dickkopf-1 is a member of a new family of secreted proteins and functions in head induction. *Nature* **391,** 357–362 (1998).
8. Caneparo, L. *et al.* Dickkopf-1 regulates gastrulation movements by coordinated modulation of Wnt/β catenin and Wnt/PCP activities, through interaction with the Dally-like homolog Knypek. *Genes Dev.* **21,** 465–480 (2007).
9. Cha, S. W., Tadjuidje, E., Tao, Q., Wylie, C. & Heasman, J. Wnt5a and Wnt11 interact in a maternal Dkk1-regulated fashion to activate both canonical and non-canonical signaling in *Xenopus* axis formation. *Development* **135,** 3719–3729 (2008).
10. Pukrop, T. *et al.* Wnt 5a signaling is critical for macrophage-induced invasion of breast cancer cell lines. *Proc. Natl Acad. Sci. USA* **103,** 5454–5459 (2006).
11. Mikheev, A. M. *et al.* Dickkopf-1 mediated tumor suppression in human breast carcinoma cells. *Breast Cancer Res. Treat.* **112,** 263–273 (2008).
12. Anastas, J. N. & Moon, R. T. WNT signalling pathways as therapeutic targets in cancer. *Nat. Rev. Cancer* **13,** 11–26 (2013).
13. Krishnan, V., Bryant, H. U. & Macdougald, O. A. Regulation of bone mass by Wnt signaling. *J. Clin. Invest.* **116,** 1202–1209 (2006).
14. Wang, F. S. *et al.* Knocking down dickkopf-1 alleviates estrogen deficiency induction of bone loss. A histomorphological study in ovariectomized rats. *Bone* **40,** 485–492 (2007).
15. Mundy, G. R. Metastasis to bone: causes, consequences and therapeutic opportunities. *Nat. Rev. Cancer* **2,** 584–593 (2002).
16. Mariz, K., Ingolf, J. B., Daniel, H., Teresa, N. J. & Erich-Franz, S. The Wnt inhibitor dickkopf-1: a link between breast cancer and bone metastases. *Clin. Exp. Metastasis* **32,** 857–866 (2015).
17. Minn, A. J. *et al.* Lung metastasis genes couple breast tumor size and metastatic spread. *Proc. Natl Acad. Sci. USA* **104,** 6740–6745 (2007).
18. Smid, M. *et al.* Subtypes of breast cancer show preferential site of relapse. *Cancer Res.* **68,** 3108–3114 (2008).
19. Labelle, M., Begum, S. & Hynes, R. O. Platelets guide the formation of early metastatic niches. *Proc. Natl Acad. Sci. USA* **111,** E3053–E3061 (2014).
20. Acharyya, S. *et al.* A CXCL1 paracrine network links cancer chemoresistance and metastasis. *Cell* **150,** 165–178 (2012).
21. Lin, E. Y., Nguyen, A. V., Russell, R. G. & Pollard, J. W. Colony-stimulating factor 1 promotes progression of mammary tumors to malignancy. *J. Exp. Med.* **193,** 727–740 (2001).
22. Qian, B.-Z. *et al.* CCL2 recruits inflammatory monocytes to facilitate breast-tumour metastasis. *Nature* **475,** 222–225 (2011).
23. Malanchi, I. *et al.* Interactions between cancer stem cells and their niche govern metastatic colonization. *Nature* **481,** 85–89 (2012).
24. Ghajar, C. M. *et al.* The perivascular niche regulates breast tumour dormancy. *Nat. Cell Biol.* **15,** 807–817 (2013).
25. Karnoub, A. E. *et al.* Mesenchymal stem cells within tumour stroma promote breast cancer metastasis. *Nature* **449,** 557–563 (2007).

26. Malladi, S. *et al*. Metastatic latency and immune evasion through autocrine inhibition of WNT. *Cell* **165,** 45–60 (2016).
27. Coffelt, S. B., Wellenstein, M. D. & de Visser, K. E. Neutrophils in cancer: neutral no more. *Nat. Rev. Cancer* **16,** 431–446 (2016).
28. Niida, A. *et al*. DKK1, a negative regulator of Wnt signaling, is a target of the β-catenin/TCF pathway. *Oncogene* **23,** 8520–8526 (2004).
29. Shi, C. & Pamer, E. G. Monocyte recruitment during infection and inflammation. *Nat. Rev. Immunol.* **11,** 762–774 (2011).
30. Talmadge, J. E. & Gabrilovich, D. I. History of myeloid-derived suppressor cells. *Nat. Rev. Cancer* **13,** 739–752 (2013).
31. Kalinski, P. Regulation of immune responses by prostaglandin E2. *J. Immunol.* **188,** 21–28 (2012).
32. Miyazono, K., Olofsson, A., Colosetti, P. & Heldin, C. H. A role of the latent TGF-β 1-binding protein in the assembly and secretion of TGF-β 1. *EMBO J.* **10,** 1091–1101 (1991).
33. Padua, D. *et al*. TGF-β primes breast tumors for lung metastasis seeding through angiopoietin-like 4. *Cell* **133,** 66–77 (2008).
34. Gleizes, P. E. *et al*. TGF-β latency: biological significance and mechanisms of activation. *Stem Cells* **15,** 190–197 (1997).
35. Lelekakis, M. *et al*. A novel orthotopic model of breast cancer metastasis to bone. *Clin. Exp. Metastasis* **17,** 163–170 (1999).
36. Boyce, B. F. & Xing, L. Functions of RANKL/RANK/OPG in bone modeling and remodeling. *Arch Biochem. Biophys.* **473,** 139–146 (2008).
37. Buijs, J. T., Stayrook, K. R. & Guise, T. A. The role of TGF-β in bone metastasis: novel therapeutic perspectives. *BoneKEy Rep.* **1,** 96 (2012).
38. Bronte, V. *et al*. Recommendations for myeloid-derived suppressor cell nomenclature and characterization standards. *Nat. Commun.* **7,** 12150 (2016).
39. Lu, D. *et al*. Dkk3 prevents familial dilated cardiomyopathy development through Wnt pathway. *Lab Invest.* **96,** 239–248 (2016).
40. Hoang, B. H. *et al*. Dickkopf 3 inhibits invasion and motility of Saos-2 osteosarcoma cells by modulating the Wnt-β-catenin pathway. *Cancer Res.* **64,** 2734–2739 (2004).
41. Krupnik, V. E. *et al*. Functional and structural diversity of the human Dickkopf gene family. *Gene* **238,** 301–313 (1999).
42. Mao, B. & Niehrs, C. Kremen2 modulates Dickkopf2 activity during Wnt/LRP6 signaling. *Gene* **302,** 179–183 (2003).
43. Li, L., Mao, J., Sun, L., Liu, W. & Wu, D. Second cysteine-rich domain of Dickkopf-2 activates canonical Wnt signaling pathway via LRP-6 independently of dishevelled. *J. Biol. Chem.* **277,** 5977–5981 (2002).
44. Fatima, S. *et al*. Dickkopf 4 (DKK4) acts on Wnt/β-catenin pathway by influencing β-catenin in hepatocellular carcinoma. *Oncogene* **31,** 4233–4244 (2012).
45. Niehrs, C. Function and biological roles of the Dickkopf family of Wnt modulators. *Oncogene* **25,** 7469–7481 (2006).

METHODS

Constructs and reagents. Human *DKK1* was cloned into pMSCV-puro (Clontech). *JUN*, IκbαM (without the amino-terminal 122 amino acids), ΔC-LEF1 (without the carboxy-terminal 94 amino acids), *DKK2*, *DKK3*, *DKK4*, *SFRP2* and murine *Dkk1* were cloned into pLenti-easy (ABM). Human ΔN-TCF4 (without the N-terminal 53 amino acids), ΔN-CTNNB1 (without the N-terminal 41 amino acids), *PTGS2* and *RELA* were cloned into pLVX (Clonetech). Human *WNT5A* was cloned into pcDNA3.1 (Thermo Fisher Scientific). For *DKK1* and *LTBP1* knockdown, the annealed sense and antisense shRNA oligonucleotides were cloned into the BglII and HindIII sites of pSuper-Retro-puro/-hygro (Oligo Engine) as previously described[46], with the following target sequences: 3′-GGAATAAGTACCAGACCATTG-5′ (*DKK1* KD1); 3′-GGATCTCTTGGAATGACAA-5′ (*DKK1* KD3); 3′-CCGTTGAATACCGCCTTGAAT-5′ (*LTBP1* KD1); 3′-GATGACCTGTGTCGATGTAAA-5′ (*LTBP1* KD2). For *PTGS2* knockdown, the annealed sense and antisense shRNA oligonucleotides were cloned into the EcoRI and AgeI site of pLKO.1 (Addgene), with the following target sequences: 3′-GCTGAATTTAACACCCTCTAT-5′ (*PTGS2* KD1) and 3′-CCATTCTCCTTGAAAGGACTT-5′ (*PTGS2* KD2). The NF-κB luciferase reporter vector contains three repeats of the GGAATTTCCG NF-κB-responsive element in the backbone of pGL3-basic (Promega). All primers for qRT-PCR and ChIP analysis are listed in Supplementary Table 4. All of the antibodies used in western blotting, immunofluorescent staining, immunohistological staining and flow cytometry are listed in Supplementary Table 5. Chemicals and recombinant proteins, as well as the corresponding concentrations used in *in vitro* and *in vivo* assays, are listed as below: DKK1 (100 ng ml^{-1} or as noted, 120-30, Peprotech), WNT3A (50 ng ml^{-1}, 5036-WN-010, R&D Systems), XAV939 (5 μM for *in vitro* assay and 25 mg ml^{-1} for mouse injection, S1180, Selleckchem), SP600125 (2 μM for *in vitro* assay and 20 mg ml^{-1} for mouse injection, S1460; Selleckchem), BAY11-7082 (5 μM, S2913, Selleckchem), SB431542 (2 μM for *in vitro* assay and 10 mg ml^{-1} for mouse injection, S1067; Selleckchem), celecoxib (30 μM for *in vitro* assay and 5 mg kg^{-1} for mouse injection, S1261, Selleckchem), KN-93 phosphate (60 μM; S6423, Selleckchem), Gö 6850 (4 μM; S7208, Selleckchem), BAPTA-AM (10 μM, S7534, Selleckchem), EHop-016 (8 μM, S7319, Selleckchem), cyclosporin A (4 μM, S2286, Selleckchem), PGE_2 (3 μM, sc-201225, Santa Cruz), mIL-6 (406-ML, R&D Systems), GM-CSF (315-03-5, Peprotech), M-CSF (315-02-50, Peprotech) and RANKL (315-11-10, Peprotech). MDA-MB-231 and its derivatives were obtained from J. Massague (Memorial Sloan Kettering Cancer Center, New York, USA)[2,17]. MCF10 and 4T1 serial cell lines were obtained from F. R. Miller (Wayne State University, Michigan, USA)[47,48]. The murine breast cancer cells from C57BL/6J MMTV/PyMT mice were derived directly from the primary tumours, thus requiring no further authentication. All cell lines were tested as mycoplasma free.

Western blot. Cultured cells were rinsed with pre-cooled PBS and lysed by lysis buffer (50 mM Tris-HCl, 150 mM NaCl, 1% Nonidet P-40, 0.5% sodium deoxycholate, 0.1% SDS with phosphatase and protease inhibitors) at 4 °C for 15 min, followed by centrifugation at 17,000*g* for 15 min. The supernatants were collected, quantified and denatured for western blot analysis. For cytoplasmic/nuclear protein extraction, cells were rinsed with PBS, scraped down and collected by centrifugation at 900*g* for 5 min. Cell pellets were washed twice by Buffer A (10 mM HEPES, 10 mM KCl, 0.5 mM dithiothreitol (DTT) and phosphatase and protease inhibitors). Cell pellets were further lysed by Buffer A with 1% Nonidet P-40 and centrifuged at 17,000*g* for 15 min. The supernatants were saved as cytoplasmic proportion. The nuclear pellets were washed three times by Buffer A with 1% Nonidet P-40 and subjected to Buffer B (20 mM HEPES, 20% glycerol, 500 mM KCl, 0.2 mM EDTA, 1.5 mM $MgCl_2$ and phosphatase and protease inhibitors) for 15 min, followed by centrifugation at 17,000*g* for 15 min. Supernatants were collected as the nuclear proportion. All representative images of western blots were obtained from at least three successful repeats.

Mouse experiments. Female BALB/c, athymic and NOD–SCID mice aged 6–8 weeks were used in all animal experiments. Orthotropic, intravenous and intracardiac injections were performed as previously described[46]. Briefly, 1×10^5, 1×10^5 and 2×10^5 cells were injected into the fat pad, left ventricle and tail vein for primary tumours, bone metastasis and lung metastasis, respectively. Celecoxib (5 mg kg^{-1}) and dimethylsulfoxide (DMSO) control was injected i.p. daily since the day of cancer cell injection for 5 weeks. SP600125 (20 mg kg^{-1}), SB431542 (10 mg kg^{-1}), XAV939 (25 mg kg^{-1}) and DMSO control were injected i.p. daily from day 14 post implantation until euthanization. Before drug treatment, mice were randomly regrouped to ensure equal average tumour sizes among groups with different treatment conditions. For macrophage and neutrophil depletion assay, mice received two initial shots (100 μl per mouse) of PBS or clodronate liposomes (5 mg ml^{-1}) every three days before cancer cell injection and followed by weekly maintenance shots (200 μl per mouse). RB6-8C5 (Bio X Cell, BE0075), 1A8 (Bio X Cell, BE0075-1) and rat IgG control (I4131, Sigma) were i.p. injected (0.1 mg per mouse) twice a week. BLI was acquired with a NightOWL II LB983 Imaging System (Berthold). Osteolytic area was measured by X-ray radiography with a Faxitron instrument (Faxitron Bioptics) as previously described[46] and quantified by ImageJ (NIH). No statistical method was used to predetermine the sample sizes. All mice with successful injection were included for further analyses. Investigators were not blinded to outcome assessment. All animal studies were conducted according to the guidelines for the care and use of laboratory animals and were approved by the Institutional Biomedical Research Ethics Committee of Shanghai Institutes for Biological Sciences.

FACS analysis and Giemsa staining of stromal components in lung metastases. Mice were euthanized at week 5–8 post transplantation and lung metastases were harvested. Stromal cells in lung metastases were analysed by flow cytometry as previously reported[20]. Briefly, lung metastases were picked, minced and further digested by 1% (w/w) Dispase (17105-041, Invitrogen) and 5 mg ml^{-1} Collagenase Type III (LS004182, Worthington) at 37 °C for 1 h. Red blood cells were lysed with RBC lysis reagent (555899, BD Pharmingen). FcR was blocked by a CD16/CD32 antibody (2.4G2, BD Life Sciences) at the concentration of 0.5 mg per million cells before antibody staining. Antibodies were diluted for staining according to the manufacturer's instructions. Flow cytometry was performed by a Gallios (Beckman Coulter) FACS system and quantified by the FlowJo software. All representative results of FACS analysis were from at least three or the annotated numbers of repeats. After FACS sorting, resuspended cells were made into smears, air-dried, fixed in methanol and stained by Rapid Wright–Giemsa Staining Solution (E607315-00001, Sangon Biotech) following the instructions from the manufacturer.

Mass-spectrum analysis of cancer cell secretome. The procedure of mass-spectrum secretome analysis was previously described[49]. Briefly, CM of denoted cancer cell lines were harvested, concentrated with the Ultra-15 centrifugal filter devices with the 3-kD cutoff (Millipore) and quantified by the Bradford method. In-gel digestion was conducted and the resultant peptides were used to perform nano LC-MS/MS experiments on the MDLC system (Michrom Bioresources) coupled with a Thermo Finnigan 2D linear ion trap mass spectrometer (LTQXL, Thermo). The reproducibility and genome-scale analysis of bone metastasis secretome data have been discussed previously[49]. Subcellular localization of the identified proteins was defined as previously described[49], and extracellular proteins including secreted and plasma membrane proteins were subjected to further analyses.

Active RHOA and RAC1 pulldown assays. Cancer cells reaching 80–90% confluence were rinsed once with pre-cooled PBS and then lysed. Cell lysate was centrifuged at 17,000*g* at 4 °C for 15 min. The supernatant was used for active RHOA and RAC1 pulldown assay with kits (Pierce, 16116 and 16118) following the manufacturer's instructions.

Two-chamber migration assay of macrophages and CD11b$^+$Gr-1$^+$ myeloid cells. Macrophages derived from murine bone marrow were differentiated as previously reported[50]. Briefly, femur and tibia were dissected out, bone marrow cells were flushed and red blood cells were lysed. The above cells were then cultured on Transwell inserts (1.5×10^5 per insert) in macrophage differentiation medium (10% heat-inactivated FBS, 30% L929 CM, 60% RPMI 1640) for seven days with medium refreshment every three days. Gr-1$^+$ myeloid cells were also differentiated *in vitro* as previously reported[51]. Briefly, bone marrow cells were flushed, and red blood cells were lysed cultured in RPMI 1640 medium with 10% heat-inactivated FBS, 10 ng ml^{-1} GM-CSF and 40 ng ml^{-1} IL-6 for four days with medium supplement every three days. For migration assays, 2×10^5, 1.5×10^5 and 1×10^6 THP-1, bone marrow-derived macrophages and Gr-1$^+$ myeloid cells in RPMI 1640 were added to the upper chamber and a 1:1 mixture of cancer cell CM and RPMI 1640 was added to the lower chamber as the chemo-attractant. For THP-1 and Gr-1$^+$ myeloid cells, migrated cells in the lower chamber were counted after 16 h (THP-1) or 3 h (Gr-1$^+$ myeloid cells). For primary macrophages, after 6 h of migration the membranes of inserts were stained by 0.1% crystal violet (w/v) and the purple region was quantified by ImageJ (NIH).

Immunofluorescent staining. Lungs of mice were dissected out at the designated time points and rinsed with pre-chilled PBS. Tissues were fixed in 4% PFA, dehydrated by 30% sucrose PBS solution overnight, embedded in OCT (4583, Sakura) on dry ice and stored at −80 °C. Lungs were sectioned to 14 μm thickness, blocked and permeated in 5% donkey serum (017-000-121, Jackson ImmunoResearch) in 0.1% Triton X-100 containing PBS, followed by primary antibody incubation overnight. DAPI (10236276001, Roche) staining was performed at room temperature for 5 min at the concentration of 1 μg ml^{-1}. Finally, sections were mounted (S3023, Dako) and observed by the Cell Observer Microscopy System (Zeiss). For immunofluorescent staining of cultured cells, cells were seeded on cover slides, fixed and permeated by 4% PFA and 0.1% Triton X-100 PBS solution for 15 min at room temperature. The cover slides were then blocked in 5% FBS,

DOI: 10.1038/ncb3613

2% BSA, 2% glycine and 0.1% Tween-20 PBS solution for 30 min. Primary and secondary antibodies were diluted in 0.5% BSA, 0.5% glycine and 0.1% Tween-20 PBS solution and incubated overnight at 4 °C and 1 h at 37 °C, respectively. DAPI staining, mounting and observation were performed as described above. All representative images were obtained from at least three successful repeats.

Chromatin immunoprecipitation. The chromatin immunoprecipitation (ChIP) assay for the *PTGS2* and *LTBP1* promoters by JUN and RELA was conducted as previously described[52]. HeLa cells were transfected with HA-JUN or HA-RELA 48 h before ChIP. Cells were crosslinked by 1% formaldehyde for 10 min and neutralized by 0.125 M glycine for 5 min at room temperature with gentle shaking. Cells were then rinsed, trypsinized and lysed with cytoplasmic lysis buffer (5 mM PIPES, 85 mM KCl, 0.5% NP-40 and protease inhibitors, pH 8.0) on ice for 10 min, followed by centrifugation at 4,700*g* for 5 min to collect nuclei. Nuclei were lysed by nuclei lysis buffer (50 mM Tris-HCl, 10 mM EDTA, 1% SDS and protease inhibitors, pH 8.1) on ice for 10 min. With the addition of dilution buffer (0.01% SDS, 1.1% Triton X-100, 1.2 mM EDTA, 16.7 mM Tris-HCl, 167 mM NaCl, pH 8.0), nuclei were sonicated until the genomic DNA size was between 500 base pairs and 1 kilobase. Cell debris was removed by centrifugation at 14,000*g* for 10 min. A proportion of supernatant was set aside as input, and the remaining solution was divided equally into two halves for IgG (sc-2027 X, Santa Cruz) and HA (sc-805 X, Santa Cruz) immunoprecipitation overnight, respectively. Pre-blocked protein A beads (17-0469-01, GE Healthcare) were added to the solution for 3 h with gentle inversions. The beads were washed by IP dialysis buffer (2 mM EDTA, 50 mM Tris-HCl and 0.2% sarkosyl, pH 8.0) twice and IP wash buffer (100 mM Tris-HCl, 500 mM LiCl, 1% NP-40 and 1% deoxycholic acid, pH 9.0) four times, and genomic DNA was eluted twice by IP elution buffer (50 mM $NaHCO_3$ and 1% SDS) at 67 °C. Eluted genomic DNA as well as input genomic DNA was de-crosslinked by 0.3 M NaCl, RNA was digested with 10 mg ml^{-1} RNase A (RB-473, Sangon Biotech) and proteins were digested by 0.2 mg ml^{-1} proteinase K (PB0451, Sangon Biotech) at 67 °C for 4 h. The DNA was precipitated with ethanol, purified and used as qPCR templates.

Luciferase assay. HeLa or SCP28 cells were transfected with the denoted constructs and treated with designated chemicals or cytokines for 24 h. Afterwards, cells were rinsed once with PBS and lysed by luciferase lysis buffer (2 mM EDTA, 20 mM DTT, 10% glycerol, 1% Triton X-100 and 25 mM Tris-base, pH 7.8) at room temperature for 1 h with shaking. The resultant lysate was subjected to firefly (25 mM glycylglycine, 15 mM potassium phosphate, 15 mM $MgSO_4$, 2 mM ATP, 10 mM DTT and 1 mM D-luciferin, pH 7.8) and *Renilla* (0.5 M NaCl, 1 mM EDTA, 0.1 M potassium phosphate, 0.04% BSA and 2 μM coelenterazine, pH 7.4) luciferase assay buffer, respectively. *Renilla* luciferase activity reads were used for normalization.

Quantification of circulating tumour cells. Murine blood was drawn through the left ventricle of the heart with 15 U ml^{-1} heparin as an anticoagulant. Red blood cells were lysed by RBC lysis buffer and the cell solution was centrifuged at 400*g* at 4 °C for 5 min. Cell pellets were resuspended and cells from the same amount of blood were seeded into 6-well plates under the selection of 2 mg ml^{-1} neomycin because 4T1.2 tumour cells gained neomycin resistance during the establishment of stable transfectants. After culturing for approximately two weeks, cells were fixed in 4% neutral paraformaldehyde and stained by 0.1% (w/v) crystal violet. Alternatively, genomic DNA was extracted and 100 ng gDNA was taken for qPCR to quantify the neomycin-resistant gene, which was detectable only in cancer cells.

Osteoclastogenesis assays. Primary bone marrow osteoclastogenesis was conducted with bone marrow harvested from 4- to 7-week-old BALB/c mice essentially as previously described[46], except that 25 ng ml^{-1} RANKL was supplied into the culture medium. CM from cancer cells was mixed with α-MEM at a 1:3 ratio for osteoclast differentiation. Various inhibitors and recombinant proteins were used to treat the cancer cells prior to CM harvest, or administrated directly into the CM–α-MEM mixture, as specified for each experiment. TRAP staining was performed with the tartrate-resistant acid phosphatase kit (Sigma 387A) as previously described[46].

Clinical analysis. Embedded primary tumour specimens and serum samples of breast cancer were obtained from Qilu Hospital of Shandong University, with informed patient consent and the approval from Institutional Review Boards. DKK1, LTBP1 and PTGS2 protein levels in the primary tumours were analysed with immunohistochemistry staining. For each sample, DKK1 was scored as negative and positive, and LTBP1 and PTGS2 were scored as negative (0), low (1), medium (2) or high (3) according to the staining intensities. Serum samples were pre-treated according to the manufacturer's instructions and analysed with ELISA kits for DKK1 (DKK100, R&D Systems), PGE_2 (KGE004B, R&D Systems), DKK2 (SEB033Hu, USCN), DKK3 (ab100502, Abcam) and DKK4 (ab100503, Abcam). Among the 164 serum samples analysed with DKK1 ELISA, 161 samples with confirmed ER, PR and HER2 information were used for subtype analysis. The median serological DKK1 level of all samples was used as the cutoff to classify the 102 samples with bone- and lung-metastasis information into two groups for Kaplan–Meier survival analysis. Among these 102 samples, 3 with relapse in both lungs and bone were removed from analysis of DKK1 levels in patients with organ-specific metastasis. The study is compliant with all relevant ethical regulations regarding research involving human participants.

Statistics and reproducibility. All data except box plots are presented as mean ± s.d. For data comparison with ≥3 experimental groups, ANOVA was performed first to assess the overall difference among groups. If differences existed, pair-wise comparisons with multi-comparison correction of *P* values were performed with Dunnett's test (multiple comparisons against the same control) or Holm's test (other types of multiple comparisons) to assess the significance of between-group differences. Repeated measures ANOVA was used to assess the difference between data sets with time series measurements, including growth curves of tumour sizes, metastasis BLI signals or cell proliferation. Log-rank test was used for survival analyses of mice and patients. Two-tailed Student's *t*-test without equal variation assumption was used to assess other *in vitro* or *in vivo* data. Statistical analyses were performed with Microsoft Excel and Stata. *P* values less than 0.05 were considered as significant. The experiments shown in Figs 1b, 2a,e, 3a,d, 4h,j, 5a,f, 6a–e and 7g and Supplementary Figs 1f, 2b–e,i–l, 3a,g–i,k,l, 4a–e, 5b,e–h,j and 7d are representatives of three or otherwise indicated independent experiments performed with similar results.

Data availability. The mass-spectrum data of breast cancer cell line secretome were deposited in ProteomeXchange with the primary accession code PXD007227.

Statistics source data for Figs 2e,f, 3b,c,e–g, 4a,c,f–g,i,k, 5d–h, 6f,g and 7d,f and Supplementary Figs 1c,h,j–k, 2c,j,n, 3b,c,f,h,i,m, 4f,i, 5d,i,l, 6a, 7a,f and 8a,e have been provided as Supplementary Table 6. All other data supporting the findings of this study are available from the corresponding author on reasonable request.

46. Wang, Y. *et al.* DLC1-dependent parathyroid hormone-like hormone inhibition suppresses breast cancer bone metastasis. *J. Clin. Invest.* **124,** 1646–1659 (2014).
47. Aslakson, C. J. & Miller, F. R. Selective events in the metastatic process defined by analysis of the sequential dissemination of subpopulations of a mouse mammary tumor. *Cancer Res.* **52,** 1399–1405 (1992).
48. Santner, S. J. *et al.* Malignant MCF10CA1 cell lines derived from premalignant human breast epithelial MCF10AT cells. *Breast Cancer Res. Treat.* **65,** 101–110 (2001).
49. Jin, L. *et al.* Differential secretome analysis reveals CST6 as a suppressor of breast cancer bone metastasis. *Cell Res.* **22,** 1356–1373 (2012).
50. Weischenfeldt, J. & Porse, B. Bone marrow-derived macrophages (BMM): Isolation and applications. *CSH Protoc.* **2008** (2008) pdb prot5080.
51. Di Mitri, D. *et al.* Tumour-infiltrating Gr-1$^+$ myeloid cells antagonize senescence in cancer. *Nature* **515,** 134–137 (2014).
52. Liang, Y. *et al.* Epigenetic activation of TWIST1 by MTDH promotes cancer stem-like cell traits in breast cancer. *Cancer Res.* **75,** 3672–3680 (2015).

nature cell biology

DOI: 10.1038/ncb3613

In the format provided by the authors and unedited.

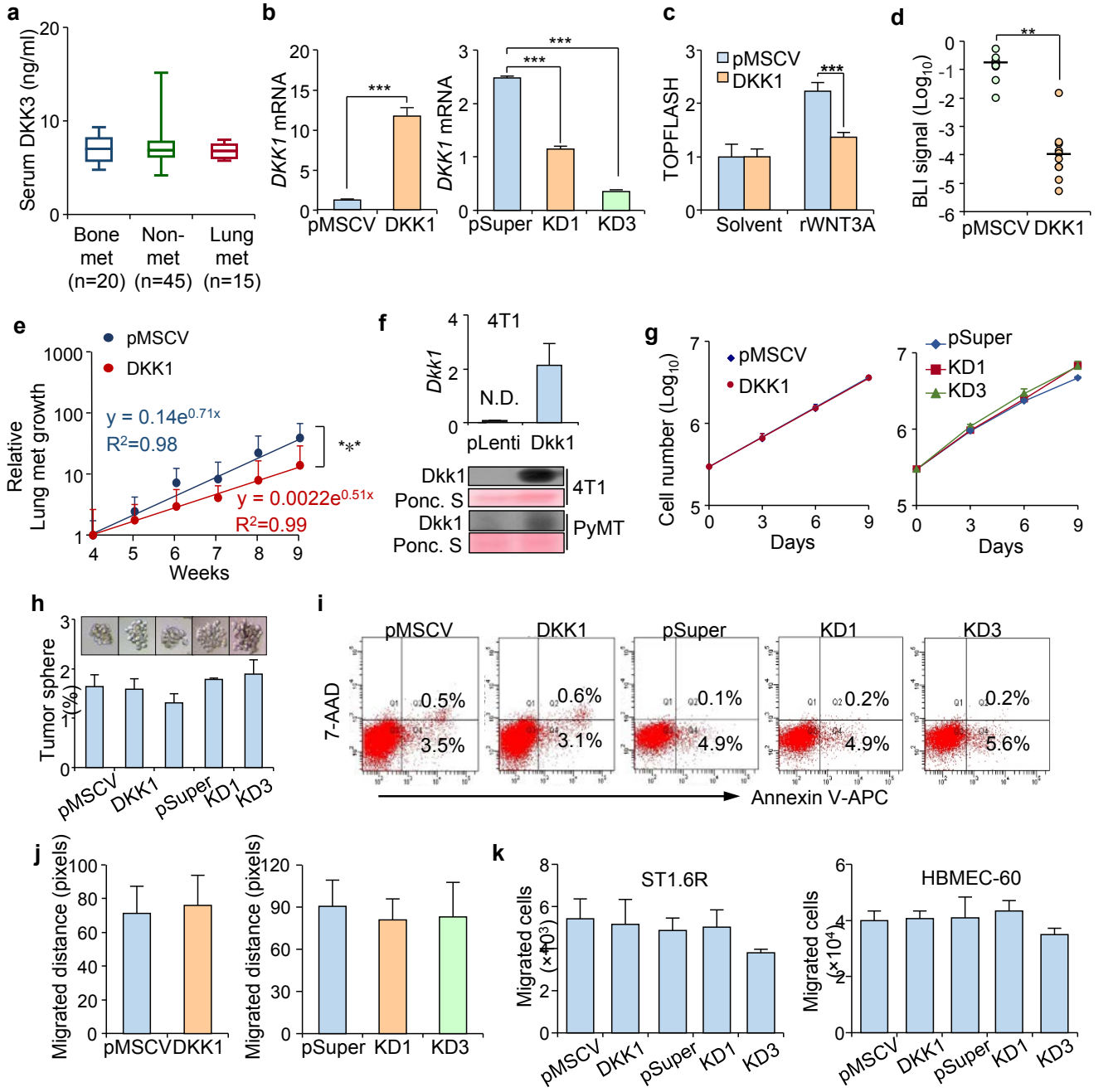

Supplementary Figure 1 Analyses of the roles of *DKK1* in lung metastasis and intrinsic malignant properties of cancer cells. (**a**) Serological DKK3 levels in Qilu breast cancer patients with different metastatic status. DKK2 and DKK4 were undetected in the majority (>96%) of serum samples. (**b**) mRNA analyses to validate *DKK1* overexpression and knockdown (KD) in SCP28 cells ($n = 3$ biologically independent samples per group). (**c**) TOPFLASH luciferase activity in HeLa with or without recombinant WNT3A (rWNT3A) treatment to validate *DKK1* overexpression ($n = 6$ biologically independent samples per group). (**d**) BLI of lung metastasis by SCP28 with or without *DKK1* overexpression 7 days after intravenous injection ($n = 10$ mice per group). (**e**) Growth curve of lung metastasis by SCP28 from week 4 to 9 ($n = 10$ mice per group). (**f**) Validation of murine *Dkk1* overexpression in 4T1 and the MMTV-PyMT-derived primary cancer cells ($n = 3$ biologically independent samples per group). (**g-k**) Analysis of *in vitro* cell growth (**g**, $n = 4$ biologically independent samples per group), tumor sphere formation (**h**, $n = 3$ biologically independent samples per group), cell apoptosis (**i**), wound-healing migration (**j**, $n = 13$ and 7 biologically independent samples per group for the left and right panel, respectively), and trans-endothelium invasion across lung-derived ST1.6R or bone-derived HBMEC-60 endothelial cells (**k**, $n = 3$ biologically independent samples per group) after *DKK1* overexpression in SCP28. $^*P<0.05$, $^{**}P<0.01$, $^{***}P<0.001$ by repeated measures ANOVA (**e**) or Student's t test (others). Unprocessed original scans of blots are shown in Supplementary Fig. 9. Box plots display values of minimum, first quartile, median, third quartile, and maximum. Bar graphs are shown as mean ± SD.

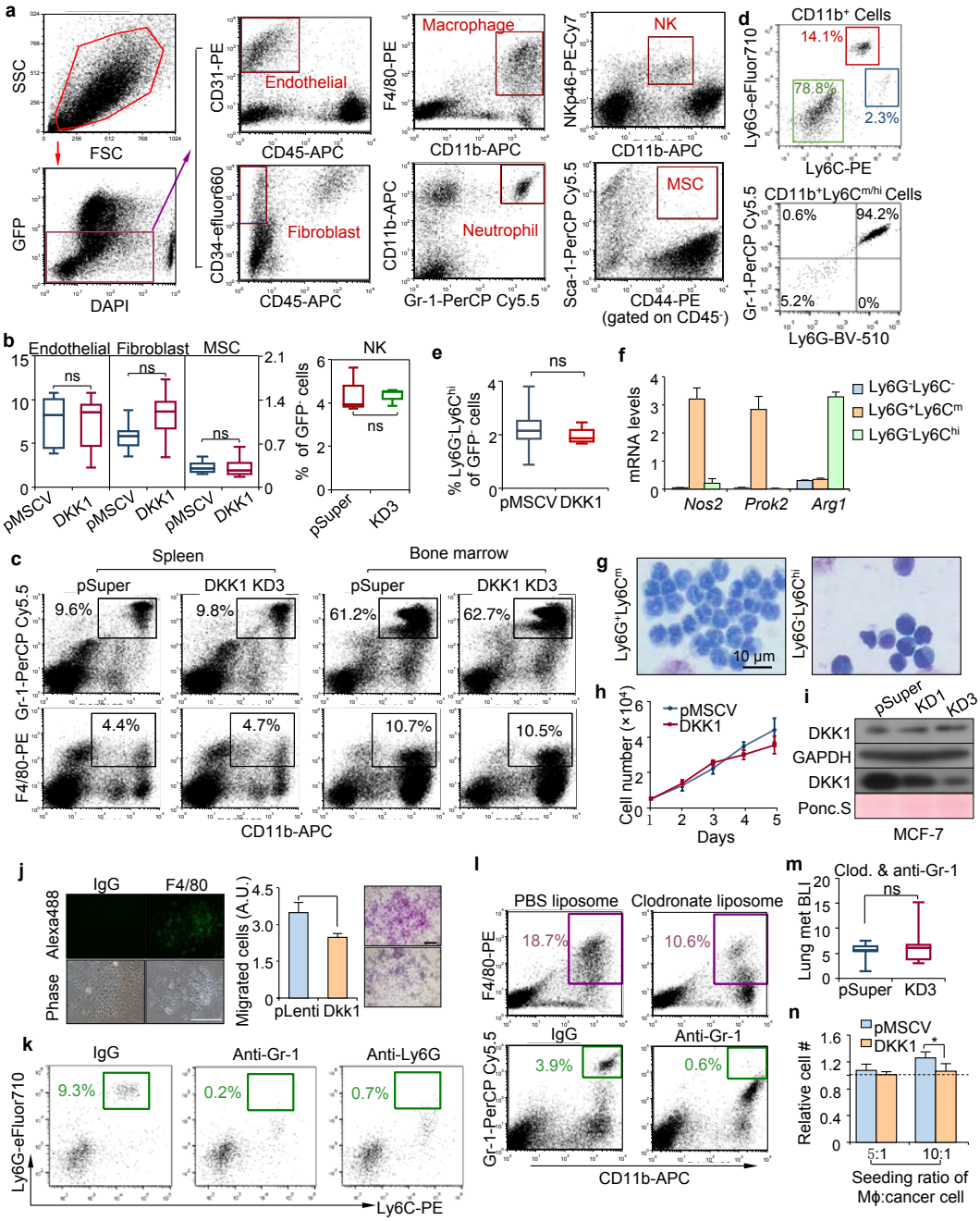

Supplementary Figure 2 DKK1 suppresses macrophage and neutrophil recruitment in lung metastases. (**a**) Workflow of flow cytometry for stromal content of lung metastases. Cancer cells were transfected with GFP and GFP$^-$ cells were gated as host cells. (**b**) Proportions of endothelial cells, fibroblasts, mesenchymal stem cells (MSCs) and natural killer (NK) cells in stroma of lung metastases with *DKK1* overexpression or knockdown ($n = 8$ and $n = 3$ biologically independent samples in the left and right panel, respectively). (**c**) Analyses of CD11b$^+$Gr-1$^+$ myeloid cells and macrophages in spleen and bone marrow of mice injected with SCP28. (**d**) Upper, the CD11b$^+$ cells in lung metastases were stained with antibodies against Ly6G (1A8) and Ly6C (HK1.4). Lower, the CD11b$^+$Ly6C$^{m/hi}$ cells in lung metastases were sequentially stained with antibodies against Ly6G (1A8) and Gr-1 (RB6). (**e**) CD11b$^+$Ly6G$^-$Ly6C^{hi} cell contents in SCP28 lung metastases. (**f**) Expression of granulocytic and monocytic markers in different CD11b$^+$ cell subsets. $n = 4$ biologically independent samples per group. (**g**) Giemsa staining of CD11b$^+$Ly6G$^+$Ly6C^m and CD11b$^+$Ly6G$^-$Ly6C^{hi} cells in lung metastases. (**h**) Growth of THP-1 cultured with CM of control or *DKK1*-overexpressing SCP28 ($n = 3$ biologically independent samples). (**i**) *DKK1* knockdown in MCF7. (**j**) Recruitment of bone marrow-derived macrophages by CM of control or *Dkk1*-overexpressing 4T1 ($n = 3$ biologically independent samples). The cell identity is validated by F4/80 immunofluorescent staining (left). Scale bar, 50 μm. (**k,l**) Validation of macrophage and neutrophil clearance in lung metastases by clodronate liposome and anti-Gr-1 (RB6-8C5) or anti-Ly6G (1A8). (**m**) Lung metastasis BLI quantitation of control and *DKK1* knockdown SCP28 in mice treated with both clodronate liposome and RB6-8C5 ($n = 5$ mice per group). (**n**) *In vitro* growth of control and *DKK1*-overexpressing SCP28, when co-cultured with different amount of bone marrow-derived macrophages ($n = 3$ biologically independent samples). $^*P<0.05$, $^{**}P<0.01$, $^{***}P<0.001$; ns, not significant, by Student's t test. Statistical source data for **c** are provided in Supplementary Table 6. Unprocessed original scans of blots are shown in Supplementary Fig. 9. Box plots display values of minimum, first quartile, median, third quartile, and maximum. Bar graphs are shown as mean ± SD.

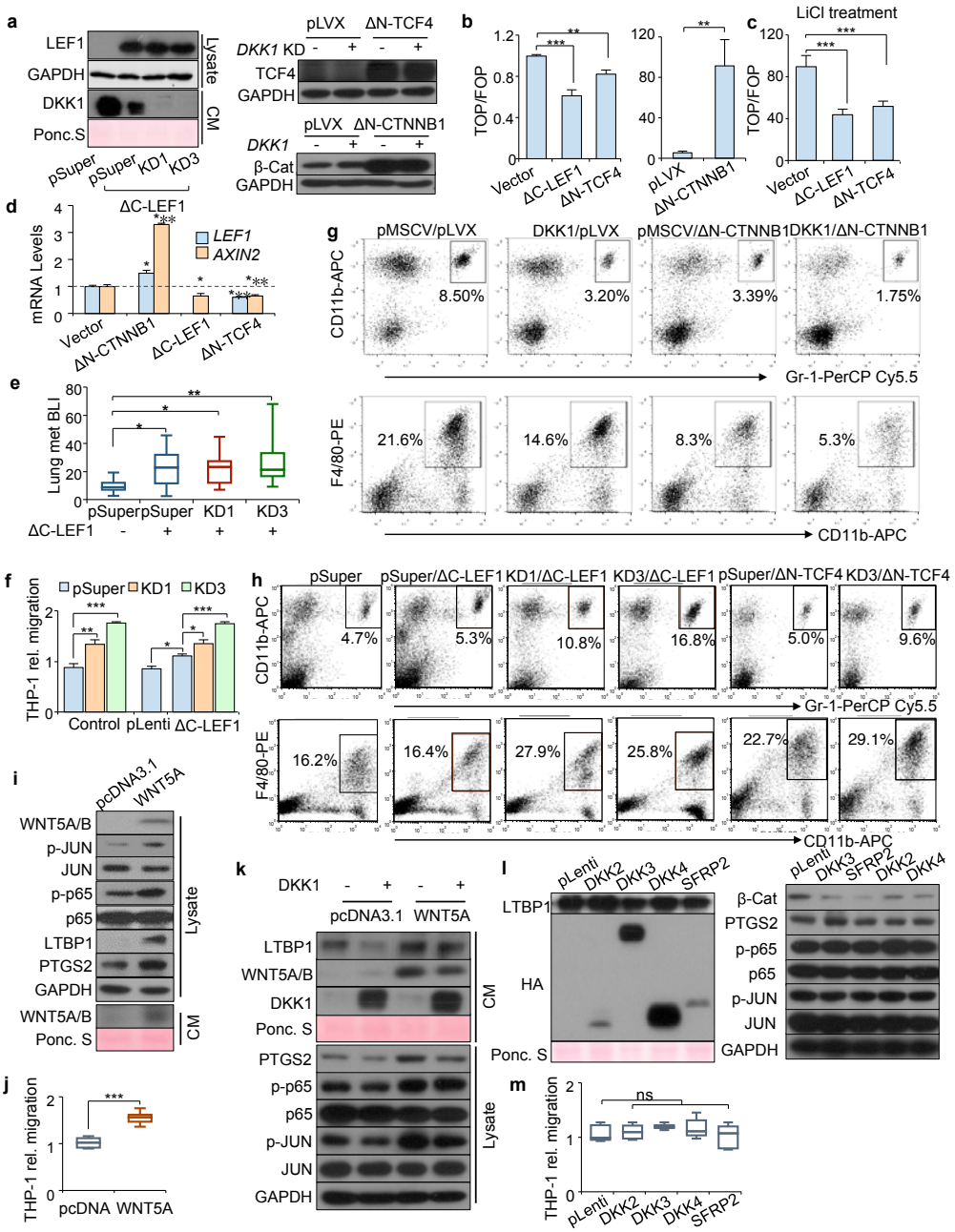

Supplementary Figure 3 The role of DKK1 in immunocyte suppression is mediated by regulating non-canonical WNT signaling pathway. (**a**) ΔC-LEF1 (left), ΔN-TCF4 (upper right) and ΔN-CTNNB1 (lower right) overexpression in SCP28 with *DKK1* knockdown or overexpression. (**b-d**) The regulatory function of ΔC-LEF1, ΔN-TCF4 and ΔN-CTNNB1 on canonical WNT signalling was validated by TOP/FOP reporter ratios at the basal status (**b**, $n = 4$ and $n = 6$ biologically independent samples for the left and right panel, respectively) or after LiCl induction (**c**, $n = 6$ biologically independent samples per group), or the changes in mRNA levels of WNT target genes *LEF1* and *AXIN2* in HeLa cells. (**d**, $n = 3$ biologically independent samples). (**e**) SCP28 Lung metastasis of intravenously injected SCP28 with *DKK1* knockdown and ΔC-LEF1 ($n = 9$ mice per group). **(f)** THP-1 migration induced by CM of SCP28 with *DKK1* knockdown and ΔC-LEF1 ($n = 8$ biologically independent samples per group). (**g-h**) Representative cell sorting results for macrophage and $CD11b^{+}Gr\text{-}1^{+}$ myeloid contents in lung metastases by SCP28 with *DKK1* overexpression and/or ΔN-CTNNB1 (**g**), or SCP28 with *DKK1* knockdown and ΔC-LEF1 or ΔN-TCF4 (**h**). (**i**) *WNT5A* overexpression in SCP28 and the upregulation of downstream non-canonical WNT signaling (p65 and JUN), and PTGS2 and LTBP1. (**j**) THP-1 migration recruited by CM of *WNT5A*-overexpressing SCP28 ($n = 8$ biologically independent samples per group). (**k**) The effects of *DKK1* and *WNT5A* dual overexpression on PTGS2 and LTBP1 expression, JUN and p65 phosphorylation. (**l-m**) The effects of expressing other WNT inhibitory ligands, DKK2-4 and SFRP2, on PTGS2 and LTBP1 expression (**l**) and THP-1 migration (**m**, $n = 7$ biologically independent samples per group). $^{*}P<0.05$, $^{**}P<0.01$, $^{***}P<0.01$, by ANOVA followed by Dunnett's (**b,c,e,f**), or Student's t test (others). Statistical source data for **h** are provided in Supplementary Table 6. Unprocessed original scans of blots are shown in Supplementary Fig. 9. Box plots display values of minimum, first quartile, median, third quartile, and maximum. Bar graphs are shown as mean ± SD.

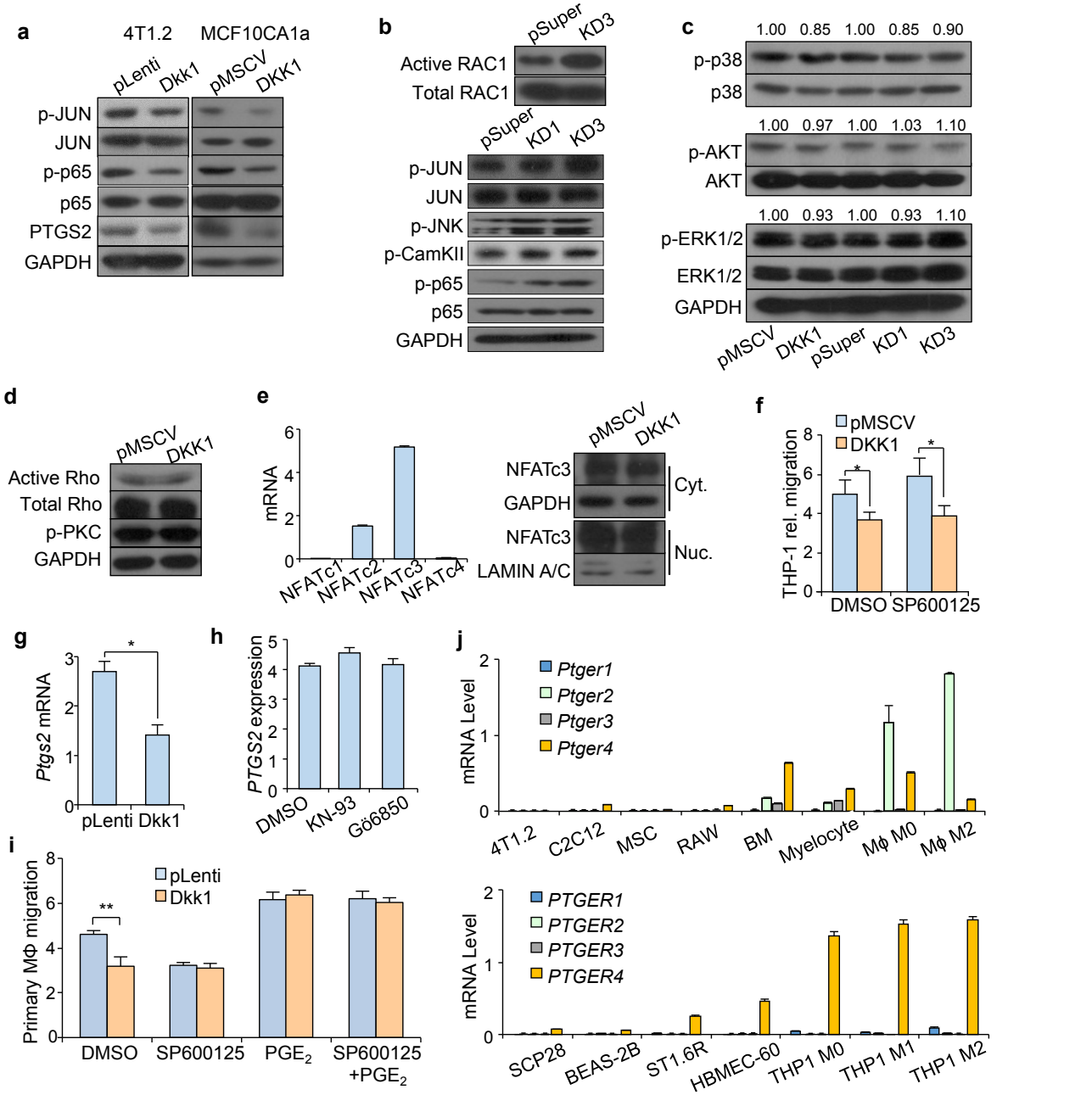

Supplementary Figure 4 DKK1 suppresses immunocyte recruitment by regulating the RAC1-JNK-PTGS2 axis. (**a**) JUN and p65 phosphorylation and PTGS2 expression after *DKK1* overexpression in 4T1.2 and MCF10CA1a. (**b**) RAC1 activation and JUN, JNK, CamKII and p65 phosphorylation after *DKK1* knockdown in SCP28. (**c-d**) ERK1/2, AKT, PKC, p38 phosphorylation and Rho activation after *DKK1* overexpression or knockdown in SCP28. (**e**) The effect of DKK1 on NFAT signaling in SCP28. Shown are the expression levels of various NFAT family members in SPC28 (left, $n = 3$ biologically independent samples per group), and the cytoplasmic and nuclear proportion of the mainly expressed NFATc3 after *DKK1* overexpression. (**f**) THP-1 recruitment was not affected by direct administration of SP600125 into CM from control or *DKK1*-overexpressing SCP28 cells ($n = 8$ biologically independent samples per group). (**g**) *Ptgs2* mRNA level after *Dkk1* overexpression in 4T1.2 ($n = 3$ biologically independent samples per group). (**h**) *PTGS2* expression was not affected by inhibitors of PKC (Gö6850) and CaMKII (KN-93) in SCP28 ($n = 3$ biologically independent samples per group). (**i**) Primary murine macrophage recruitment by 4T1 CM pre-treated with SP600125 or directedly administrated PGE_2 ($n = 3$ biologically independent samples per group). (**j**) The expression of *PTGER*1-4 in various murine cell lines and bone marrow (BM)-derived cells (left), and in various human cell lines (right). $n = 3$ biologically independent samples per group. Mφ M0 and M2 refer to naïve macrophages derived from murine bone marrow, and those further differentiated by mIL13 treatment (25 ng/ml, 72 h); THP-1 M0, M1 and M2 refer to naïve, M1 and M2 macrophages derived from THP-1, by treatments of PMA (30 ng/ml, 72 h), PMA (72 h)+ LPS (100 ng/ml, 66 h, 6h after PMA treatment) and PMA (6h)+ IL13 (25 ng/ml, 66h, 6h after PMA treatment). $^{**}P<0.01$, $^{*}P<0.05$ by Student's t test. Unprocessed original scans of blots are shown in Supplementary Fig. 9. Box plots display values of minimum, first quartile, median, third quartile, and maximum. Bar graphs are shown as mean ± SD.

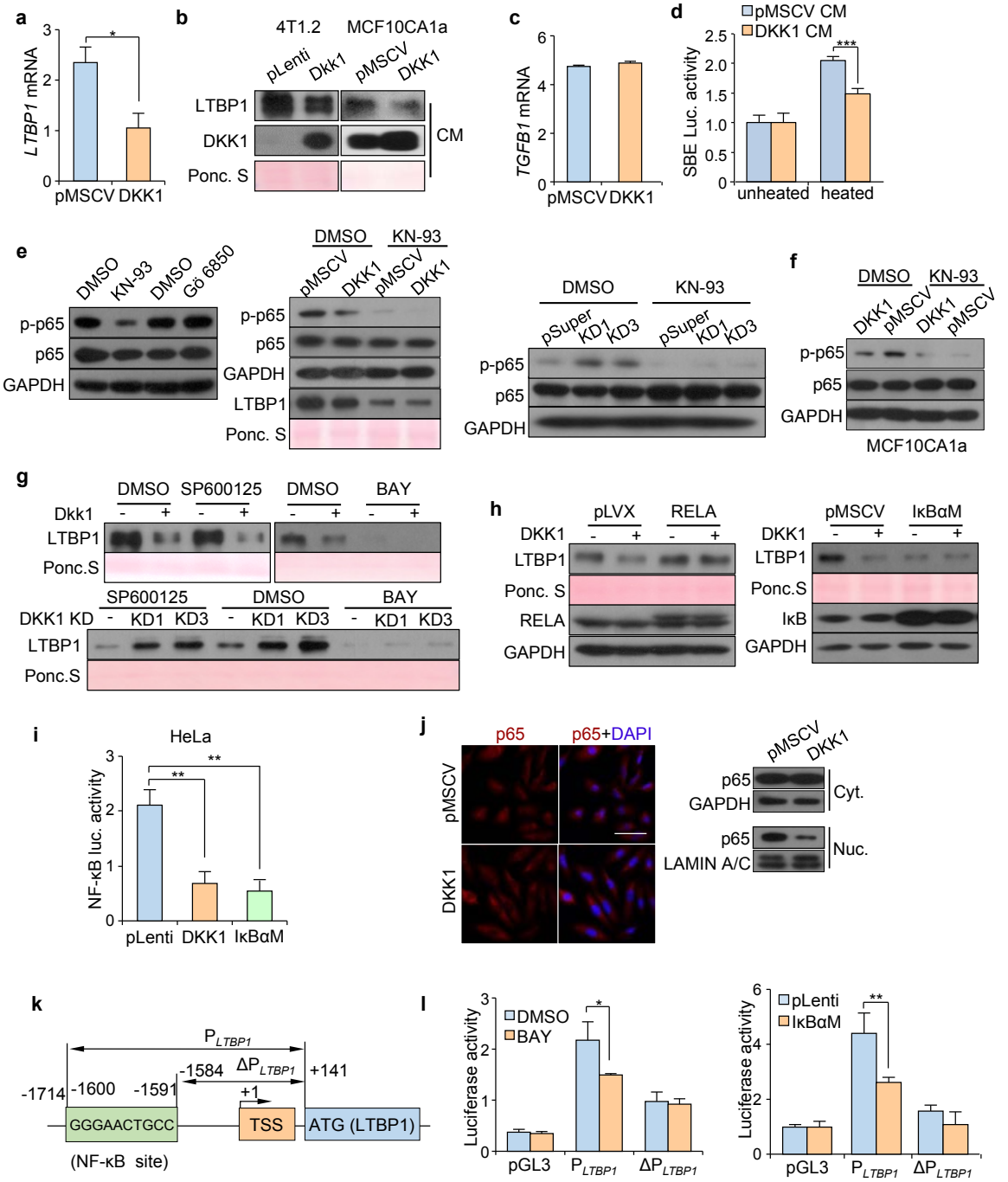

Supplementary Figure 5 DKK1 regulates LTBP1 and TGFβ bioavailability by suppressing NF-κB. (**a**) LTBP1 mRNA level in SCP28 after *DKK1* overexpression ($n = 3$ biologically independent samples per group). (**b**) LTBP1 secretion level in 4T1.2 and MCF10CA1a after *DKK1* overexpression ($n = 3$ biologically independent samples per group). (**c**) TGFβ1 mRNA level in SCP28 after *DKK1* overexpression. $n = 3$ biologically independent samples per group. (**d**) SBE activity ($n = 5$ biologically independent samples per group) in HeLa cells treated by CM from *DKK1*-overexpressing SCP28, with or without heating activation of latent TGFβ1 in the CM. (**e**) The effects of PKC (Gö6850) and CaMKII (KN-93) inhibitors on p65 phosphorylation and LTBP1 expression in SCP28 (left), or SCP28 with *DKK1* overexpression (middle) or knockdown (right). (**f**) The effects of KN-93 on p65 phosphorylation in MCF10CA1a with *DKK1* overexpression. (**g**) The effects of SP600125 and BAY11-7082 on *LTBP1* expression in *Dkk1*-overexpressing 4T1.2 (upper), and in SCP28 with *DKK1* knockdown (lower). (**h**) The effect of RELA (p65) and IkBαM on LTBP1 expression in SCP28 with *DKK1* overexpression. (**i**) NF-κB responsive reporter activity in HeLa cells transfected with *DKK1* or IκBαM ($n = 4$ biologically independent samples per group). (**j**) p65 nuclear localization analyses in SCP28 after *DKK1* overexpression by immunofluorescent staining (left) and subcellular fractionation (right). (**k**) Scheme of *LTBP1* promoter reporter construction for NF-κB binding site analysis. The sequence of predicted NF-κB binding site was shown. (**l**) Luciferase activity of *LTBP1* wild-type or truncated (ΔP_{LTBP1}, without the NF-κB binding site) promoter in HeLa treated with NF-κB inhibitor BAY11-7082 or IkBαM ($n = 4$ biologically independent samples per group). *P<0.05, **P<0.01, ***P<0.01, by ANOVA followed by Dunnett's test (**i**) or Student's t test (others). Unprocessed original scans of blots are shown in Supplementary Fig. 9. Bar graphs are shown as mean ± SD.

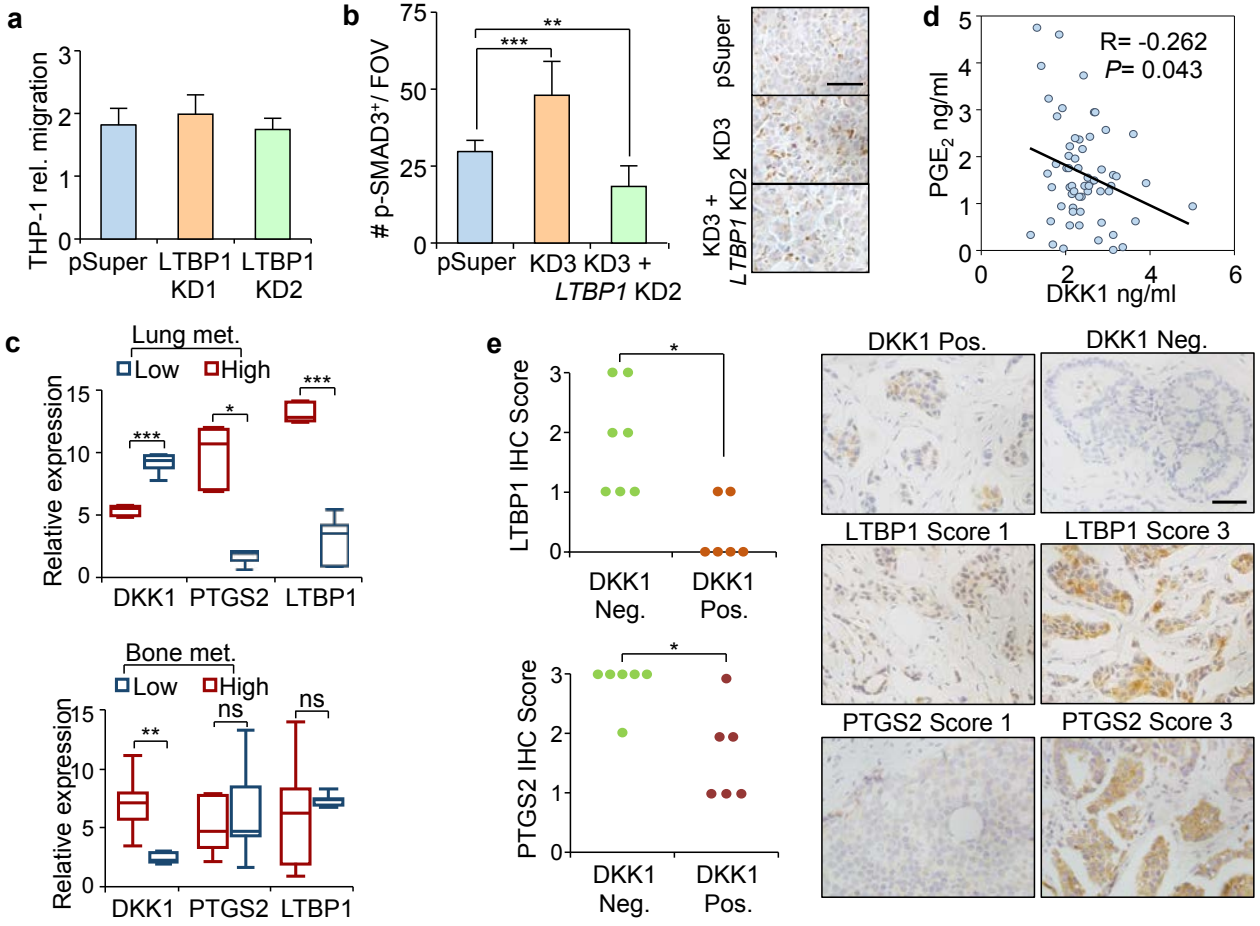

Supplementary Figure 6 PTGS2 and LTBP1 mediate the role of DKK1 in lung metastasis. (**a**) SCP28 CM-induced THP-1 recruitment was not affected by *LTBP1* knockdown ($n = 8$ biologically independent samples per group). (**b**) IHC analysis of p-SMAD3 in lung metastases by intravenously injected SCP28 with *DKK1* KD3 and *LTBP1* KD2 ($n = 12$ samples from 3 mice per group). Scale bar, 50 μm. (**c**) Expression of *DKK1*, *PTGS2* and *LTBP1* in breast cancer cells with varied lung (upper) and bone (lower) metastatic capabilities. $n = 8$ and 14 biologically independent samples for the upper and lower panel, respectively. (**d**) Serological DKK1 and PGE_2 levels of the Qilu cohort patients ($n = 60$ patient serum samples). (**e**) Immunohistochemistry staining of DKK1, LTBP1 and PTGS2 in the Qilu cohort ($n = 13$ individual primary tumors per group). Shown on right are the representative images of DKK1, LTBP1 and PTGS2 IHC staining. Scale bars, 50 μm. $^{*}P<0.05$, $^{**}P<0.01$, $^{***}P<0.001$ by ANOVA followed by Dunnett's test (**b**), Pearson correlation analysis (**d**) or Student's t test (others). Box plots display values of minimum, first quartile, median, third quartile, and maximum. Bar graphs are shown as mean ± SD.

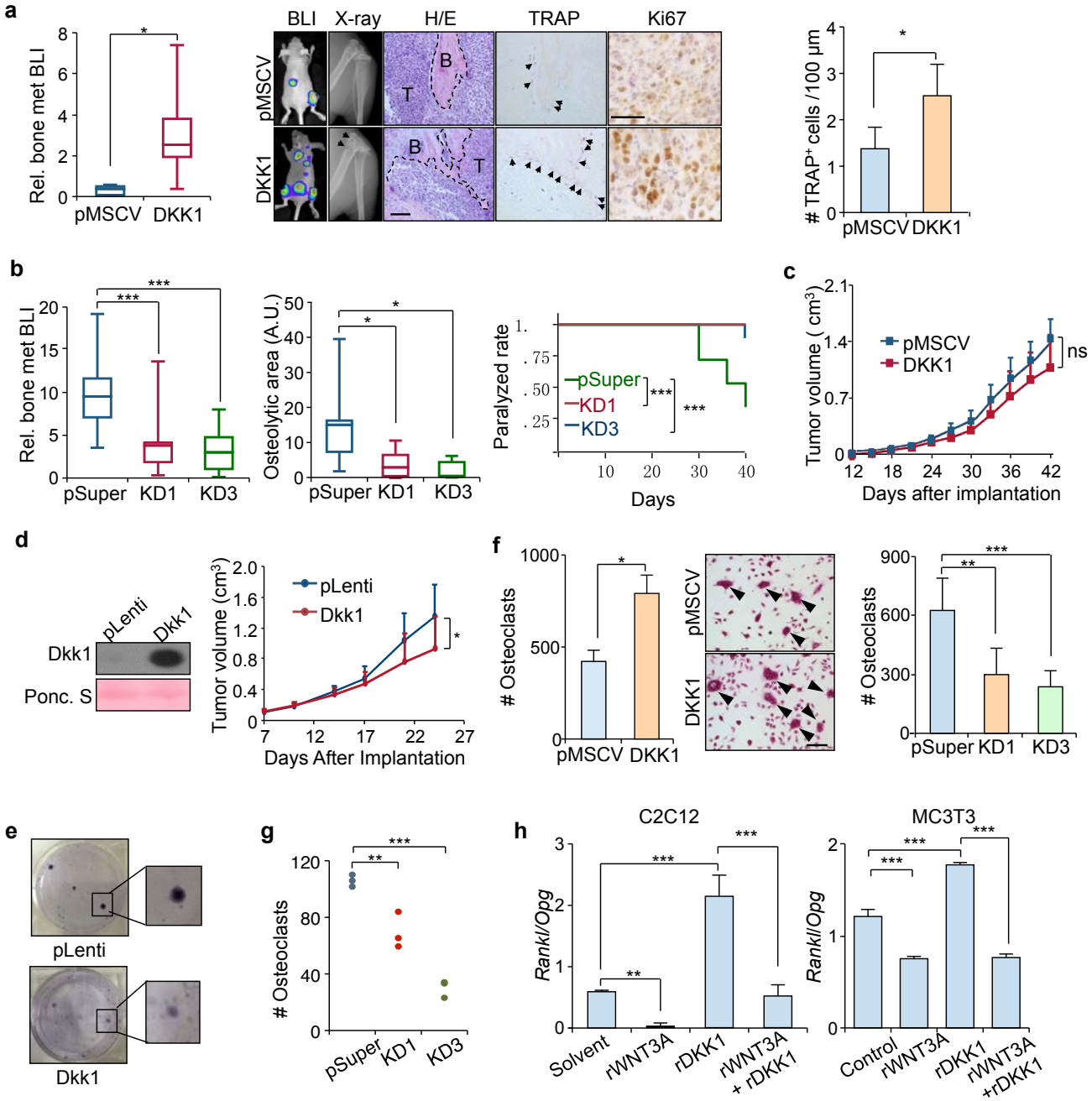

Supplementary Figure 7 DKK1 promotes osteoclastogenesis by regulating osteoblast canonical WNT signaling. (**a**) Intracardiac injection of SCP28 with *DKK1* overexpression ($n = 10$ mice per group). Shown are bioluminescent imaging (BLI) analyses (left), representative BLI, X-ray, H/E, TRAP and Ki-67 staining of bone metastases (middle), and $TRAP^+$ cell quantification along tumor-bone interface (right, $n = 24$ samples from 3 mice per group). middle, arrows point to overt bone lesions and $TRAP^+$ cells; letters B and T denote bone and tumor areas. (**b**) Intracardiac injection of SCP28 cells with *DKK1* knockdown ($n = 10$ mice per group). Shown are BLI and X-ray analyses (left), osteolytic area quantification (middle), and paralysis rates (right). (**c**) Primary tumor growth rate of orthotopically injected SCP28 cells with *DKK1* overexpression in NOD/SCID mice ($n = 10$ mice per group). (**d,e**) Orthotopic injection of 4T1.2 cells with *Dkk1* overexpression in BALB/c mice for bone and lung metastasis ($n = 8$ mice per group). Shown are validation of *Dkk1* overexpression and 4T1.2 primary tumor growth (**d**), colony-formation analyses of cells in animal blood to quantitate the circulating cancer cells (**e**). (**f**) Osteoclastogenesis of primary bone marrow cultured in CM of SCP28 with *DKK1* overexpression and knockdown ($n = 4$ biologically independent samples per group). Shown in the middle are representative images of TRAP staining. Arrow heads denote mature osteoclasts. (**g**) Osteoclastogenesis of primary bone marrow cultured in CM of MCF7 with *DKK1* knockdown. $n = 3$ biologically independent samples for each group. (**h**) *Rankl/Opg* expression ratio of C2C12 and MC3T3 treated with recombinant human DKK1 and/or WNT3A proteins. $n = 4$ biologically independent samples for each group. Scale bars, 50 µm. $^*P<0.05$, $^{**}P<0.01$, $^{***}P<0.001$; ns, not significant, by repeated measures ANOVA (**c**, **d**), ANOVA followed by Dunnett's (**b**, **f** right panel and **g**) or Holm's test (**h**), or Student's t test (others). Statistical source data for **a** are provided in Supplementary Table 6. Unprocessed original scans of blots are shown in Supplementary Fig. 9. Box plots display values of minimum, first quartile, median, third quartile, and maximum. Bar graphs are shown as mean ± SD.

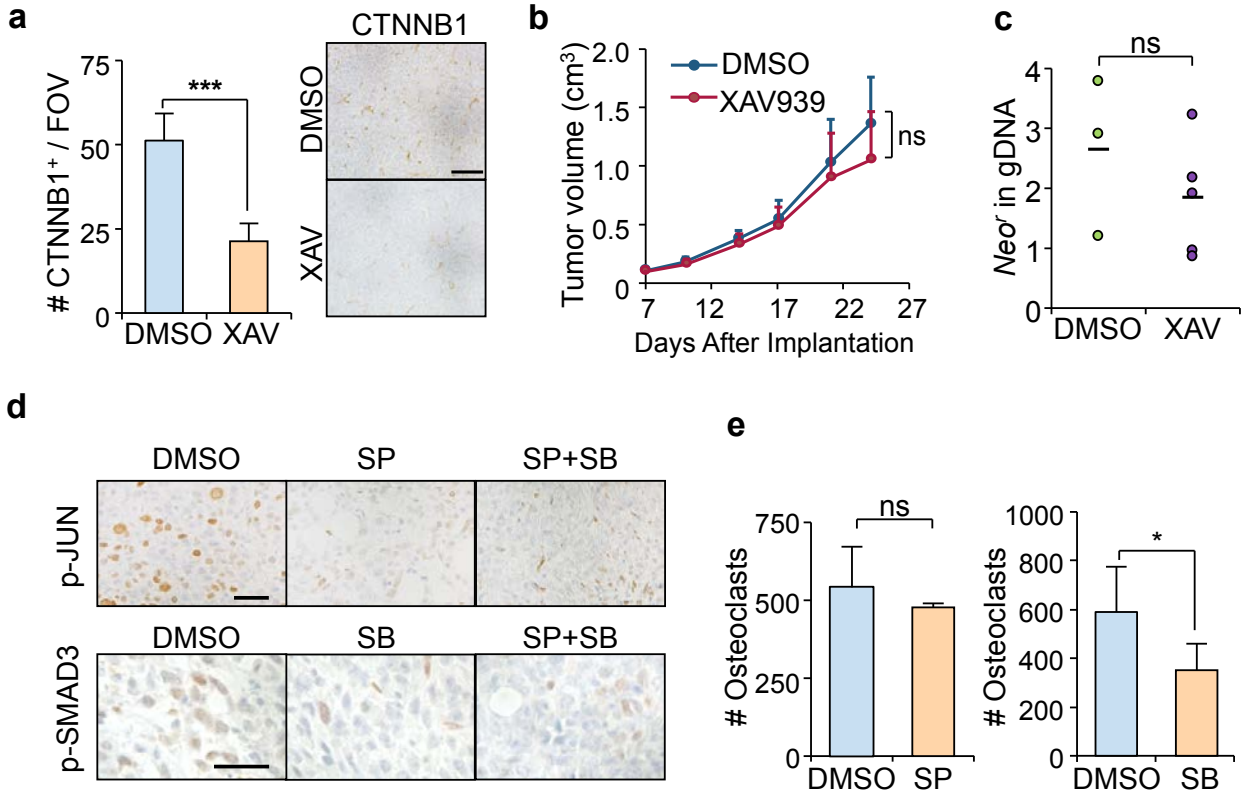

Supplementary Figure 8 The anti-metastasis effects of targeting canonical WNT or combinatory targeting of JNK and TGFβ. (**a-c**) BALB/c mice with 4T1.2 orthotopic tumors were treated with the canonical WNT inhibitor XAV939 ($n = 8$ samples from 3 mice per group). Shown were CTNNB1 IHC staining of 4T1.2 primary tumors to validate the effect of XAV939 on WNT signaling (**a**, $n = 8$ biologically independent samples per group; Scale bar, 50 μm), primary tumor growth (**b**, $n = 8$ biologically independent animals per group), and quantitation of circulating tumor cells (**c**, $n = 3$ biologically independent animals per group). Circulating tumor cells were quantitated by qPCR of the Neomycin resistant marker gene, which was used to label the cancer cells. (**d**) Phosphorylated SMAD3 and JUN IHC in 4T1.2 primary tumors to validate the effects of the inhibitors on JNK-JUN and TGFβ signaling, in BALB/c mice treated with SP600125 (SP), SB431542 (SB) or both. (**e**) Osteoclastogenesis of primary bone marrow treated with SP600125 or SB431542 ($n = 4$ and $n = 5$ biologically independent samples per group for the left and right panel, respectively). $^{*}P<0.05$, $^{***}P<0.001$, ns, not significant, by repeated measures ANOVA (b), or Student's t test (others). Bar graphs are shown as mean ± SD.

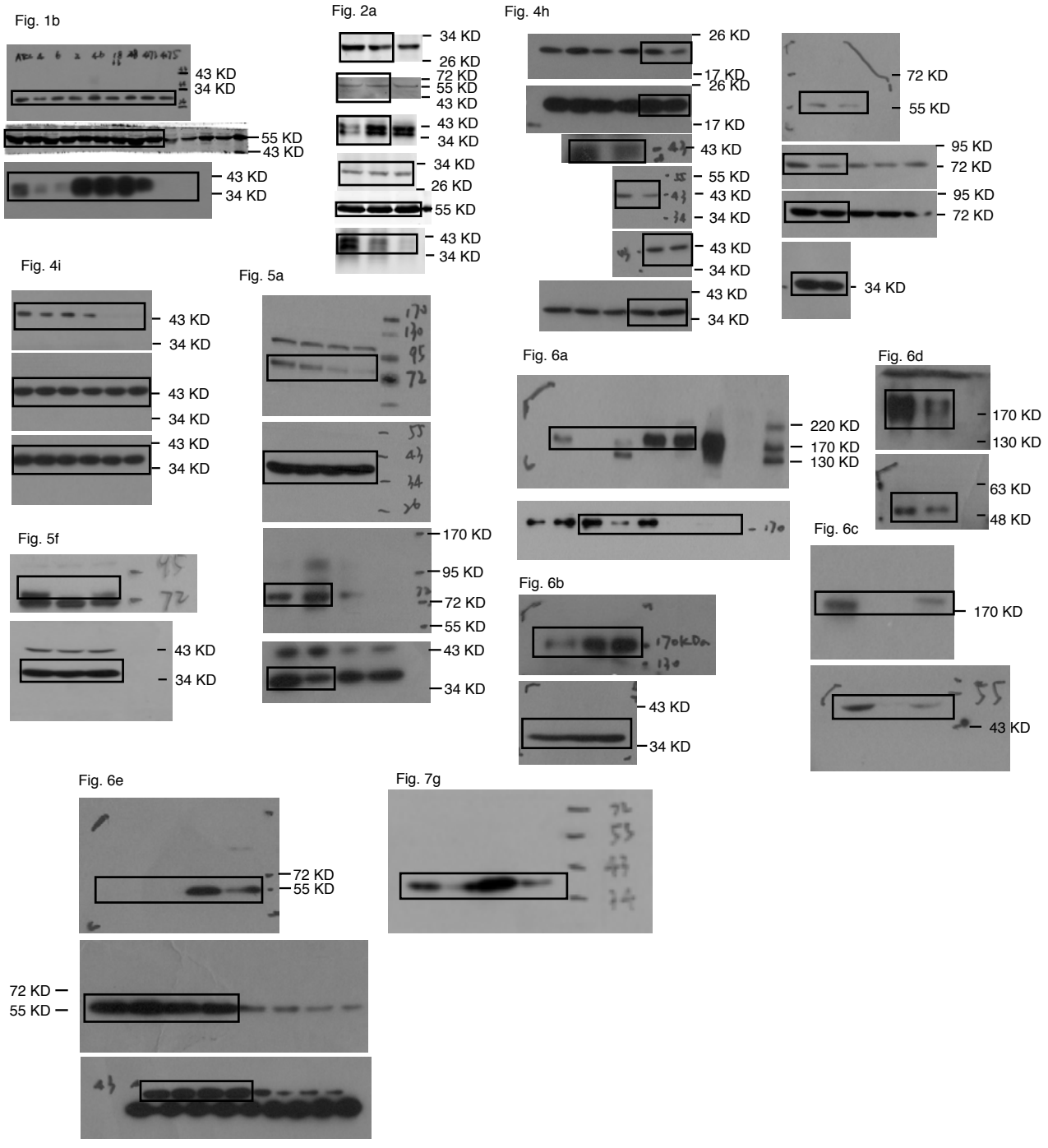

Supplementary Figure 9 Original uncropped Western blots in main and supplementary figures.

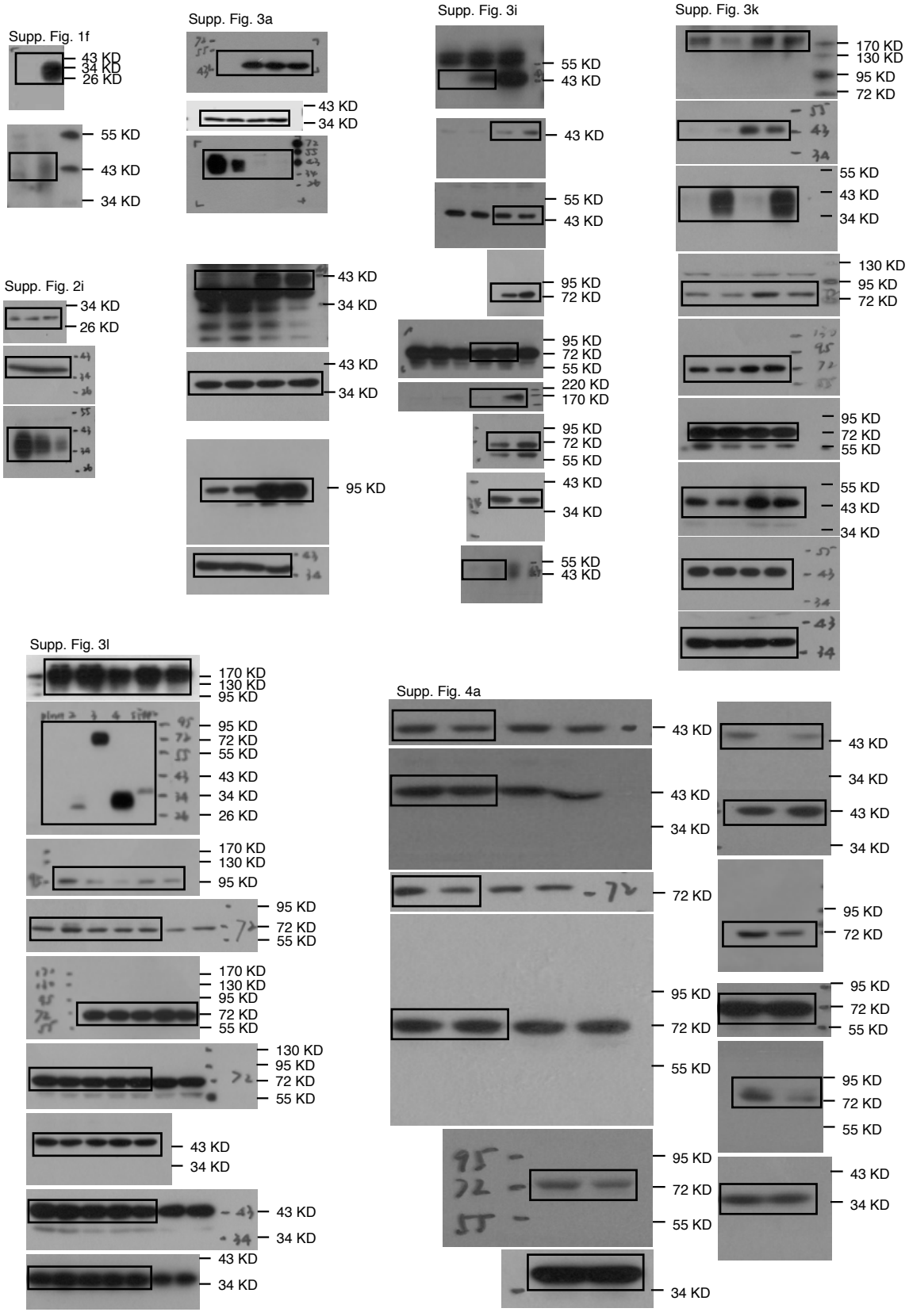

Supplementary Figure 9 Continued

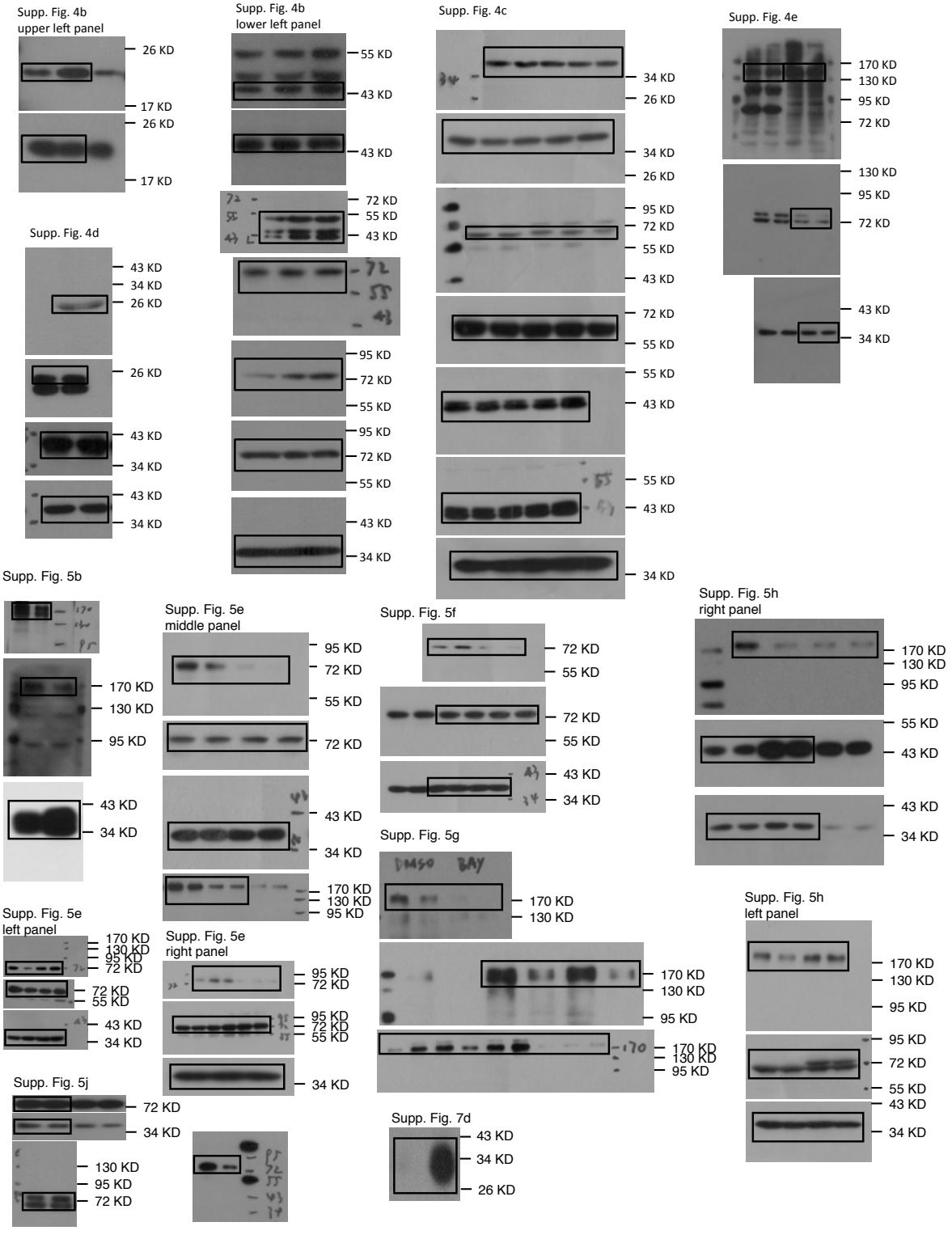

Supplementary Figure 9 Continued

Supplementary Table Legends

Supplementary Table 1 Secreted proteins associated with bone and lung metastasis.

Supplementary Table 2 DKK1-regulated secretory proteins identified by mass spectrum analysis.

Supplementary Table 3 Expression ratios of macrophage and myeloid cell recruitment-related factors in SCP28 after DKK1 overexpression.

Supplementary Table 4 Primer sequences.

Supplementary Table 5 Information of antibodies used for western blotting, IF, IHC and FACS analyses.

Supplementary Table 6 Statistics Source Data.

nature research

Corresponding author(s): Guohong Hu

☐ Initial submission ☒ Revised version ☐ Final submission

Life Sciences Reporting Summary

Nature Research wishes to improve the reproducibility of the work that we publish. This form is intended for publication with all accepted life science papers and provides structure for consistency and transparency in reporting. Every life science submission will use this form; some list items might not apply to an individual manuscript, but all fields must be completed for clarity.

For further information on the points included in this form, see Reporting Life Sciences Research. For further information on Nature Research policies, including our data availability policy, see Authors & Referees and the Editorial Policy Checklist.

Experimental design

1. Sample size

Describe how sample size was determined.

No sample size calculation is performed before conducting experiments.

2. Data exclusions

Describe any data exclusions.

No data is excluded if the experiments were successfully performed.

3. Replication

Describe whether the experimental findings were reliably reproduced.

All attempts strictly following methods were successful.

4. Randomization

Describe how samples/organisms/participants were allocated into experimental groups.

Samples or animals were allocated randomly into experimental groups.

5. Blinding

Describe whether the investigators were blinded to group allocation during data collection and/or analysis.

Investigators were not blinded to group allocation during data collection and/or analysis.

Note: all studies involving animals and/or human research participants must disclose whether blinding and randomization were used.

6. Statistical parameters

For all figures and tables that use statistical methods, confirm that the following items are present in relevant figure legends (or in the Methods section if additional space is needed).

n/a	Confirmed
☐	☒ The exact sample size (*n*) for each experimental group/condition, given as a discrete number and unit of measurement (animals, litters, cultures, etc.)
☐	☒ A description of how samples were collected, noting whether measurements were taken from distinct samples or whether the same sample was measured repeatedly
☐	☒ A statement indicating how many times each experiment was replicated
☐	☒ The statistical test(s) used and whether they are one- or two-sided (note: only common tests should be described solely by name; more complex techniques should be described in the Methods section)
☐	☒ A description of any assumptions or corrections, such as an adjustment for multiple comparisons
☐	☒ The test results (e.g. *P* values) given as exact values whenever possible and with confidence intervals noted
☐	☒ A clear description of statistics including central tendency (e.g. median, mean) and variation (e.g. standard deviation, interquartile range)
☐	☒ Clearly defined error bars

See the web collection on statistics for biologists for further resources and guidance.

Software

Policy information about availability of computer code

7. Software

Describe the software used to analyze the data in this study.	Microsoft Office Excel and Stata were used to perform statistical analyses.

For manuscripts utilizing custom algorithms or software that are central to the paper but not yet described in the published literature, software must be made available to editors and reviewers upon request. We strongly encourage code deposition in a community repository (e.g. GitHub). *Nature Methods* guidance for providing algorithms and software for publication provides further information on this topic.

Materials and reagents

Policy information about availability of materials

8. Materials availability

Indicate whether there are restrictions on availability of unique materials or if these materials are only available for distribution by a for-profit company.	All materials in this study were either available from authors or from companies listed in Method section.

9. Antibodies

Describe the antibodies used and how they were validated for use in the system under study (i.e. assay and species).	All antibodies in this study were listed in Supplementary Table 7 with names of suppliers, catalog numbers, clone numbers and dilution details for western blot, immunofluorescent staining, immunohistological staining and flow cytometry assays. The utility of these antibodies were all stated on the websites of corresponding suppliers.

10. Eukaryotic cell lines

a. State the source of each eukaryotic cell line used.	MDA-MB-231 and its derivatives were obtained from Dr. Massague. MCF10 and 4T1 serial cell lines were obtained from Dr. Miller.
b. Describe the method of cell line authentication used.	MDA-MB-231 derivatives and MCF10, 4T1 series were requested from original contributors. We made sure that the cell morphology and gene expression were not changed over the course of cell culture in our laboratory. No other authentication was performed.
c. Report whether the cell lines were tested for mycoplasma contamination.	All cell lines were tested negative for mycoplasma contamination.
d. If any of the cell lines used are listed in the database of commonly misidentified cell lines maintained by ICLAC, provide a scientific rationale for their use.	No cell lines adopted in this study is listed in the database of commonly misidentified cell lines maintained by ICLAC.

Animals and human research participants

Policy information about studies involving animals; when reporting animal research, follow the ARRIVE guidelines

11. Description of research animals

Provide details on animals and/or animal-derived materials used in the study.	Female BALB/c, athymic and NOD-SCID mice aged 6-8 weeks were used in all animal studies.

Policy information about studies involving human research participants

12. Description of human research participants

Describe the covariate-relevant population characteristics of the human research participants.	Embedded primary tumour specimens and serum samples of breast cancer were obtained from Qilu Hospital of Shandong University, with informed patient consent and the approval from Institutional Review Boards. The metastatic prognosis, survival after diagnosis and ER/PR/HER2 status were included in the clinical analysis and available upon reasonable request.

nature research

Corresponding author(s): Guohong Hu

☐ Initial submission ☒ Revised version ☐ Final submission

Flow Cytometry Reporting Summary

Form fields will expand as needed. Please do not leave fields blank.

Data presentation

For all flow cytometry data, confirm that:

☒ 1. The axis labels state the marker and fluorochrome used (e.g. CD4-FITC).

☒ 2. The axis scales are clearly visible. Include numbers along axes only for bottom left plot of group (a 'group' is an analysis of identical markers).

☒ 3. All plots are contour plots with outliers or pseudocolor plots.

☒ 4. A numerical value for number of cells or percentage (with statistics) is provided.

Methodological details

5. Describe the sample preparation.	Mice were sacrificed at week 5-8 post transplantation and lung metastases were harvested. Lung metastases were picked, minced, and further digested by 1% (w/w) Dispase (17105-041, Invitrogen) and 5 mg/ml Collagenase Type III (LS004182, Worthington) at 37 ºC for 1 h. Red blood cells were lysed with RBC lysis reagent (555899, BD Pharmingen). FcR was blocked by a CD16/CD32 antibody (2.4G2, BD Life Sciences) at the concentration of 0.5 mg/million cells before antibody staining. Antibodies were diluted for staining according to manufacturer's instructions.
6. Identify the instrument used for data collection.	Gallios, Beckman Coulter
7. Describe the software used to collect and analyze the flow cytometry data.	FlowJo was used to analyze flow cytometry data.
8. Describe the abundance of the relevant cell populations within post-sort fractions.	Post-sort fractions were subjected to the same gating strategy during sorting and the abundance of the relevant cell populations was over 95%.
9. Describe the gating strategy used.	The gating strategy was shown in Supplementary Figure 2. The FSC/SSC gating was firstly conducted to exclude those cellular fragments or multi-cellular clots with both low or high FSC/SSC reads. GFP negative stromal population was gated based on GFP-positive cancer cells. Other markers, CD11b, CD45, F4/80, Gr-1, Ly6G, Ly6C, CD34, CD44, Sca-1, CD31 and NKp46 were gated positive or negative based on the difference between the corresponding IgG control and antibody.

Tick this box to confirm that a figure exemplifying the gating strategy is provided in the Supplementary Information. ☒